DOI: 10.26599/FSHW.2026.9251033

Contents lists available at SciOpen

Food Science and Human Wellness

journal homepage: https://www.sciopen.com/journal/2097-0765

China Food Publishing Co.

Structural characterization and protective effects of an *Apostichopus japonicus*-derived fucoidan against lipopolysaccharide-induced acute lung inflammation

Yang Hu[1#], Chao-Nan Ma[2#], Qin-Bing Xue[1,3#], Xue Wang[2], Shi-Lin Song[1,3], Nuo Shen[2], Feng-Yu Liu[2], Shou-Dong Guo[1,2,3*]

[1]*College of pharmacy, Harbin University of Commerce, Harbin 150076, China.*

[2]*School of Pharmacy, Shandong Second Medical University, Weifang 261053, China.*

[3]*Engineering Research Center for Medicine, Ministry of Education, Harbin University of Commerce, Harbin 150076, China.*

ABSTRACT: Acute lung inflammation (ALI) poses a significant global health challenge. Conventional synthetic anti-inflammatory drugs often show limited efficacy against ALI and may cause side effects. Natural fucoidans exhibit promising anti-inflammatory properties, but their specific effects and mechanisms in ALI remain unclear. In this study, we characterized the structural features of *Apostichopus japonicus*-derived fucoidan **AJ2-I** using methylation analysis, 1D/2D nuclear magnetic resonance, and chemical assays. We then evaluated its anti-ALI effects in lipopolysaccharide-challenged C57BL/6J mice and human A549 cells. Structural analysis revealed that **AJ2-I** primarily consists of [→3)-Fucp-(1→] residues with C4 branching, while sulfate groups were predominantly substituted at C2 and C4 positions. Notably, this fucoidan contains unique glycosyls—→4)-β-D-GalpA-6-O-Et-(1→ and →4)-β-D-GalpA-6-OMe-(1→—distinguishing it from previously reported *A. japonicus* polysaccharides. Functionally, **AJ2-I** significantly suppressed pro-inflammatory cytokines (TNF-α, IL-6, and IL-1β) in both *in vivo* and *in vitro* models. Mechanistically, it inhibited **Toll-like receptor 2/4** to suppress **mitogen-activated protein kinase** and **phosphoinositide-3 kinase/protein kinase B** signaling pathways, thereby blocking the activation of key transcription factors, including **nuclear factor kappa-B** and **c-Jun/activator protein-1**. These findings elucidate the protective role of *A. japonicus*-derived fucoidan **AJ2-I** in ALI and uncover its underlying molecular mechanisms, supporting the potential use of fucoidans in treating lung inflammation.

Keywords: Acute inflammation; fucoidan; lipopolysaccharide; mitogen-activated protein kinase; sea cucumber; Toll-like receptor

1. Introduction

The lung not only serves as the primary organ for gas exchange in mammals but also acts as a critical immune organ, functioning as the major site of interaction for many airborne pathogens, toxicants, and allergens that cause pneumonia and other diseases[1-3]. Notably, respiratory infections or other factors (e.g., aspiration pneumonitis) can induce acute lung inflammation or injury (ALI), with its most severe form, acute respiratory distress syndrome (ARDS), representing a critical threat to human health worldwide[1,4,5]. For

Contribute equally to this article.
***Corresponding author**
SD-GUO@hotmail.com

Received 8 September 2025
Received in revised from 9 October 2025
Accepted 14 November 2025

instance, the COVID-19 pandemic, caused by severe acute respiratory syndrome coronavirus 2 (SARS-CoV-2), has affected over 180 countries and territories, infecting more than 190 million people and claiming more than 4.1 million lives worldwide[6,7]. Mechanistically, infected target cells and lymphocytes overproduce pro-inflammatory cytokines, leading to ALI and a cytokine storm driven by systemic inflammation[8].

Current pharmacological treatments for ALI fall into two categories: anti-inflammatory therapy and physiological therapy. The latter involves drugs targeting ventilation, diffusion or perfusion, while anti-inflammatory approaches are widely investigated due to the inflammatory nature of ALI/ARDS[9]. Clinically, dexamethasone (Dex), ulinastatin, prednisone, and prednisolone are commonly used for acute inflammation or allergies, including ALI, owing to their anti-inflammatory and immunomodulatory effects[5]. However, these synthetic drugs often cause side effects and exhibit limited efficacy. Despite significant advancements, no fully effective pharmacological treatment for ALI/ARDS currently exists[2,3,5,10]. The urgent need to combat ALI/ARDS demands the development of both effective preventive and therapeutic strategies.

In this context, natural products have emerged as promising candidates due to their multifaceted therapeutic properties[11,12]. Among them, natural polysaccharides exhibit notable immunomodulatory properties, capable of both enhancing immune responses by promoting inflammatory cytokine release and suppressing inflammation by inhibiting over-activated immune cells. These effects are mechanistically linked to the activation of Toll-like receptors (TLRs) and their downstream signaling pathways. The proposed mechanisms involve direct interaction, potentially via β-D-configured glycosyl residues, as well as indirect modulation through metabolites derived from the intestinal flora[13-16]. Notably, fucoidans have demonstrated significant anti-inflammatory properties[11,17-19]. The structure of *Apostichopus japonicus*-derived fucoidans differs from those isolated from other sea cucumber species, and their structural characteristics vary based on the origin and extraction method[20,21]. Notably, the efficacy of fucoidan—particularly sea cucumber-derived fucoidan—in treating lung inflammation, such as ALI, remains unclear. Lipopolysaccharide (LPS), a key component of gram-negative bacterial membranes, is a major contributor to ALI. LPS-induced lung injury models are widely recognized for their high reproducibility and relevance to human ALI[22,23]. In this study, we hypothesized that sea cucumber *A. japonicus*-derived fucoidan could mitigate LPS-induced ALI in C57BL/6J mice and A549 cells by modulating TLR signaling pathway.

2. Materials and methods

2.1 Materials

The sea cucumber *A. japonicas* was bought from a local market of Qingdao (Shandong, China). Monosaccharide and dextran standards were obtained from Sigma (St. Louis, MO, USA). LPS was bought from Solarbio (Beijing, China). Dulbecco's modified Eagle's medium (DMEM) was obtained from Gibco (CA, USA). Fetal bovine serum (FBS) was purchased from Bioexplorer Life Sciences (CA, USA). Mouse monoclonal antibodies against c-Jun N-terminal kinase (JNK), phosphoinositide-3 kinase (PI3K), and interleukin (IL)-6, and a rabbit polyclonal antibody against tumor necrosis factor α (TNF-α) were provided

by Santa Cruz (California, USA). A mouse monoclonal antibody against interleukin (IL)-1β, rabbit monoclonal antibodies against p38-mitogen-activated protein kinase (MAPK) (p38), phosphorylated p38-MAPK (p-p38), extracellular regulated protein kinase 1/2 (ERK1/2), phosphorylated ERK1/2 (p-ERK1/2), phosphorylated PI3K (p-PI3K), protein kinase B (AKT/PKB), phosphorylated AKT (p-AKT), p65-nuclear factor kappa-B (NF-κB) (p65), and phosphorylated p65-NF-κB (p-p65) were bought from Cell Signaling (MA, USA). A mouse monoclonal antibody against myeloid differentiation factor 88 (MyD88) and glyceraldehyde-3-phosphate dehydrogenase (GAPDH) were bought from Proteintech (Wuhan, China). A mouse monoclonal antibody against β-tubulin, rabbit polyclonal antibodies against TLR2, TLR4, c-Jun/activator protein-1 (AP-1), phosphorylated AP-1 (p-AP-1), β-actin, and phosphorylated MyD88 (p-MyD88) were procured from Affinity Biosciences (Jiangsu, China). A rabbit polyclonal antibody against phosphorylated JNK (p-JNK) was purchased from Signalway Antibody (USA). TLR4 inhibitor (IAXO-102) and TLR2 inhibitor (INH14) were bought from Selleck (Shanghai, China) and Shanghai Yuanye Bio-Technology Co., Ltd. (Shanghai, China). A bicinchoninic acid (BCA) assay kit and HRP conjugated secondary antibodies were obtained from CWBIO (Beijing, China). An assay kit for lactate dehydrogenase (LDH)

was purchased from Beyotime (Shanghai, China). Methyl thiazolyl tetrazolium (MTT) was provided by Solarbio (Beijing, China). The rest reagents used in this study were of analytical grade.

2.2 Isolation and purification of fucoidan

Fucoidan was extracted from *A. japonicus* using an established protocol[24,25]. Briefly, dried sea cucumber body walls were soaked overnight in water, homogenized, and suspended in 0.1 M sodium acetate buffer (pH=6.0) containing 0.25% papain, 5 mM EDTA, and 5 mM cysteine (1:20, w/v). The mixture was incubated at 60 °C with continuous stirring for 24 h, followed by centrifugation at 1,500 × g for 20 min. The supernatant was concentrated to 50% of its original volume and precipitated with two volumes of 95% ethanol (4 °C, overnight) to yield crude polysaccharides. The crude extract was deproteinized using the Sevag method[26], re-suspended in water (25 g/L), and fractionated on a Q-Sepharose™ Fast Flow column (50 × 300 mm) connected to an ÄKTA fast protein liquid chromatography (FPLC) system. Stepwise elution was performed with 0.0, 0.5, 1.0, and 2.0 M NaCl[27,28]. Carbohydrate-positive fractions were pooled, concentrated, dialyzed, and lyophilized to obtain four fractions. The AJ-2 fraction was further purified by size-exclusion chromatography on a Sephacryl S200 HR column (2.6 × 90 mm), yielding a major fucoidan fraction designated AJ-2I for subsequent experiments.

2.3 Molecular weight (Mw) and chemical component analysis

The purity and Mw of AJ-2I were analyzed by high-performance gel permeation chromatography (HPGPC) using a TOSOH TSKgel G4000PWXL column with a RID-10A refractive index detector (Shimadzu, Japan). The mobile phase consisted of 0.1 M Na_2SO_4 at a flow rate of 1.0 mL/min[29]. Total carbohydrate content was quantified by the phenol-sulfuric acid method using fucose as the standard[30]. The content of uronic acid in this study was determined using the classical carbazole-sulfuric acid method with

glucuronic acid (GlcA) as the standard[31]. Sulfate ester content was determined via the barium chloride gelatin method[32], and protein content was measured using a BCA assay kit.

2.4 Monosaccharide composition analysis

This experiment was performed following an established protocol[19,33]. Samples (5 mg) were completely hydrolyzed with 2.0 M trifluoroacetic acid (TFA) at 110 ℃ for 6 h. Residual TFA was removed through rotary evaporation under reduced pressure. The hydrolysates were then derivatized with PMP (1-phenyl-3-methyl-5-pyrazolone) and analyzed using an Agilent Eclipse XDB-C18 column (4.6 × 250 mm, 5 μm) connected to a high performance liquid chromatography (HPLC) system. The mobile phase consisted of 0.1 M phosphate-buffered saline (PBS, pH=6.7) and acetonitrile (83:17, v/v) at a flow rate of 1.0 mL/min. Monosaccharide composition was determined by comparing retention times with authentic standards and calculating relative molar ratios from peak areas.

2.5 Fourier-transform infrared (FT-IR) analysis

FT-IR spectroscopy was performed using a Thermo Scientific Nicolet iS10 spectrometer. Approximately 0.5 mg sample was homogenized with potassium bromide powder and compressed into a 1 mm pellet. Spectra were acquired in the mid-infrared range (4000-500 cm^{-1}).

2.6 Methylation analysis

This experiment was performed according to an established method[32]. Sodium methylsulfinylmethylide (SMSM) was prepared by mixing 2 mL DMSO with 200 mg NaH under nitrogen atmosphere. The pre-dialyzed and freeze-dried sample, AJ-2I, was completely dissolved in DMSO in a three-necked flask under nitrogen protection with continuous stirring. The solution was sonicated while SMSM (1:10, w/v) was added dropwise, followed by 30 min reaction at room temperature in the dark. The reaction mixture was then cooled on ice, and methyl iodide (1:10, w/v) was added dropwise. After 1 h sonication at room temperature, excess methyl iodide was removed by rotary evaporation. The product was dialyzed against tap-water and lyophilized. To ensure complete derivatization, the methylation process was repeated three times to obtain the final methylated product. The completely methylated fucoidan was fully hydrolyzed with 2.0 M TFA, reduced with sodium borodeuteride, and acetylated with acetic anhydride. The resulting methylated alditol acetates were extracted with dichloromethane, dried, and analyzed by gas chromatography-mass spectrometry (GC-MS) using a DB-225 capillary column (Agilent, USA). Data interpretation referenced the Complex Carbohydrate Research Center database.

2.7 Nuclear magnetic resonance (NMR) analysis

AJ-2I (~60 mg) was subjected to three consecutive exchanges with 99.9% D_2O. After drying, the sample was dissolved in 0.6 mL of 99.9% D_2O. Deuterated acetone was added as an internal reference standard. One-dimensional ^1H-NMR, distortionless enhancement by polarization transfer spectroscopy (DEPT), ^1H-^1H correlated spectroscopy (COSY), ^1H-^{13}C heteronuclear multiple quantum coherence spectroscopy (HMQC), ^1H-^{13}C heteronuclear multiple bond coherence spectroscopy (HMBC), and nuclear overhauser effect

spectroscopy (NOESY) experiments were carried out at 25 ℃ on a Bruker Avance III HD 600 MHz spectrometer with varying acquisition times.

2.8 Animal grouping and interventions

This study was approved by the Laboratory Animal Ethical Committee of Shandong Second Medical University (No.: 2018226) and followed the ARRIVAL and NIH guidelines for the care and use of Laboratory Animals. Twenty-five male C57BL/6J mice (~8 weeks old) were bought from Beijing HFK Bioscience Co., Ltd. (No.: SCXK (Jing) 2014-0004). After a two-week acclimation period, the mice were randomly divided into five groups (n=5 per group): blank control (BC), model (Mod), Dex (10 mg/kg), low-dosage AJ-2I (F-L, 50 mg/kg), and high-dosage AJ-2I (F-H, 200 mg/kg). Dosages were selected based on previous studies[24,34,35]. All treatments were administrated orally for 7 consecutive days. Two hours after the final dose, the BC group received PBS (0.5 mL, i.p.), while the other groups were challenged with LPS (5.0 mg/kg, 0.5 mL, i.p.). Four hours post-LPS injection, mice were euthanized for sample collection. To minimize timing-related variability, drug administration and sample collection were staggered at 30-minute intervals across groups.

To determine if the anti-inflammatory effects of AJ-2I are TLR2/4 dependent, we used the aforementioned LPS-induced mouse model. C57BL/6J mice (approximately 10 weeks old) were obtained from the animal center of Shandong Second Medical University and randomly divided into the following groups (n=6/group): a Mod group, a TLR2/4 inhibitors group (TLR2 inhibitor (5 mg/kg) + TLR4 inhibitor (3 mg/kg)), and a combination group (TLR2/4 inhibitors + AJ-2I (200 mg/kg)). The inhibitor dosages were based on established literatures[36,37]. The mice were treated strictly according to the aforementioned approaches. In accordance with the 3R principles, a separate BC group and Dex group were not established for this confirmatory experiment; instead, samples from these groups were sourced from the prior experiment for the western blotting analysis.

2.9 Hematoxylin & eosin (H & E) staining

Lung tissues were fixed in 4% paraformaldehyde for 48 h, followed by dehydration through a graded ethanol series (70-100%). After clearing, tissues were immersed in molten paraffin wax (58 ℃) and embedded into blocks. The paraffin blocks were trimmed, sectioned at 5 μm using a microtome, and floated on a warm water bath (42 ℃) to smooth wrinkles. Sections were mounted onto glass slides, dried, and baked at 60 ℃ for 50 min to enhance adhesion. Slides were dewaxed in xylene and rehydrated through a descending alcohol series (100%-70%) to water. Nuclei were stained with hematoxylin for 5 min, followed by differentiated in acid alcohol and bluing in ammonia water. Cytoplasm and extracellular matrix were counterstained with eosin (0.5% aqueous) for 3 min. Finally, slides were dehydrated through graded alcohols (70-100%), cleared in xylene, and mounted[24,32]. Histological images were captured using a SMART biomicroscope (Chongqing, China).

2.10 Cell culture and treatment

A549 cells or human umbilical vein endothelial cells (HUVECs) were seeded in 25-cm^2 flasks and maintained in DMEM supplemented with 10% FBS, 100 U/mL penicillin, and 100 μg/mL streptomycin at 37 ℃ in a humidified 5% CO_2 incubator. For the cytotoxicity assay, A549 cells or HUVECs were seeded in 96-well plates at a density of 1.0×10^4 cells per well. After 24 h of treatment with AJ-2I at concentrations of 0, 10, 20, 30, and 40 μg/mL, 20 μL of MTT solution (5.0 mg/mL) was added to each well. The plates were incubated for another 2 h to allow formazan crystal formation. Subsequently, the cells were washed three times with PBS. The formazan crystals were solubilized in DMSO, and the optical density was measured at 570 nm using a SpectraMax i3x Multi-Mode Microplate Platform (Molecular Devices, San Jose, CA, USA). Cytotoxicity was further assessed using a lactate dehydrogenase (LDH) release assay, which quantifies cell membrane damage by measuring the leakage of the cytosolic enzyme LDH. The assay was performed in accordance with the manufacturer's protocol.

Upon reaching 80% confluency, A549 cells were seeded into 6-well plates and randomly assigned to five groups: BC, Mod, Dex (1.0 μM), F-L (10 μg/mL), and F-H (40 μg/mL) groups. Following a 2-hour pretreatment with respective compounds, cells (except BC group) were stimulated with 1 μg/mL LPS[25,38,39] and incubated for an additional 24 h before sample collection. For TLR2/4 inhibition experiments, cells were pretreated with TLR2/4 inhibitors (INH14 and IAXO-102; 4.0 μg/mL) and/or F-H (40 μg/mL) prior to LPS challenge. Dosages were determined based on previous literatures[17,18,40,41].

2.11 Quantitative reverse transcription-polymerase chain reaction (RT-qPCR)

Total RNA was isolated using Trizol reagent following manufacturer's protocol. The purity and concentration of total RNA were determined by NanoDrop UV spectrophotometry (Thermo Fisher, USA). cDNA synthesis was performed using an ABI Veriti™ 96-well thermal cycler according to the manufacturer's instructions. RT-qPCR was conducted using an ABI QuantStudio3 PCR system (Waltham, MA, USA) with gene-specific primers (Table 1). The amplification protocol consisted of an initial denaturation at 95 ℃ for 10 min, followed by 40 cycles of 15 s at 95 ℃ and 1 min at 60 ℃. Gene expression was quantified using the $2^{-\Delta\Delta Ct}$ method and normalized to GAPDH[32,38].

Table 1. The primers used for the polymerase chain reaction.

Primer		Sequence (5'-3')
mGAPDH	Forward	AAGAAGGTGGTGAAGCAGGCATC
	Reverse	CGGCATCGAAGGTGGAAGAGTG
mIL-6	Forward	CTTCTTGGGACTGATGCTGGTGAC
	Reverse	TCTGTTGGGAGTGGTATCCTCTGTG
mIL-1β	Forward	CCAGGATGAGGACATGAGCA
	Reverse	CGGAGCCTGTAGTGCAGTTG
mTNF-α	Forward	ACTCCAGGCGGTGCCTATGI
	Reverse	AGTGTGAGGGTCTGGGCCAT
mTLR2	Forward	AAGATGCGCTTCCTGAATTTG
	Reverse	TCCAGCGTCTGAGGAATGC
mTLR4	Forward	ATGGCATGGCTTACACCACC
	Reverse	GAGGCCAATTTTGTCTCCACA
mPI3K	Forward	TGCAGCACAATGACTCCC
	Reverse	TTCATCGCCTCTGTTGTGCAT
mAKT	Forward	TTCACAACCAGGACCAGCAGA

	Reverse	ATCCATGAGGATCAGCTCGAAC
mERK1/2	Forward	GCCTTCCAACCTCCTGCTGAAC
	Reverse	CGTACTCTGTCAAGAACCCTGTGTG
mP38	Forward	GGCAGGAGCTGAACAAGACCATC
	Reverse	AGCAGACGCAACTCTCGGTAGG
mJNK	Forward	CGCCTTATGTGGTGACTCGCTAC
	Reverse	CTCCCATGATGCACCCAACTGAC
mP65	Forward	CTCCTGTTCATCCGACTCCC
	Reverse	AGTCAGTGCCTGTTTTACGTT
mAp-1	Forward	AGCCGCCGCACCACTTG
	Reverse	CCTTGATCCGCTCCTGAGACTC
mMyD88	Forward	TCATGTTCTCCATACCCTTGGT
	Reverse	AAACTGCGAGTGGGGTCAG
hGAPDH	Forward	ACAACTTTGGTATCGTGGAAGG
	Reverse	GCCATCACGCCACAGTTTC
hIL-6	Forward	GGTGTTGCCTGCTGCCTTCC
	Reverse	GTTCTGAAGAGGTGAGTGGCTGTC
hIL-1β	Forward	GCGGCATCCAGCTACGAATCTO
	Reverse	AACCAGCATCTICCTCAGCTTGTC
hTNF-α	Forward	AGCTGGTGGTGCCATCAGAGG
	Reverse	TGGTAGGAGACGGCGATGCG
hTLR2	Forward	CTGTGCTCTGTTCCTGCTGA
	Reverse	GATGTTCCTGCTGGGAGCTT
hTLR4	Forward	GCCTTCTCAGCAGGAACACT
	Reverse	TGTTGCTTCCTGCCAATTGC
hPI3K	Forward	AGATCGCTCTGGCCTCATTG
	Reverse	AGCCAGTTCAGAAGGGCATC
hAKT	Forward	TCAAAGAAGTCAAAGGGGCTGC
	Reverse	CTCCTTCACAATAGCCACGTC
hERK1/2	Forward	AACAGGCCCATCTTTCCAGG
	Reverse	TCAGCATTTGGGAACAGCCT
hP38	Forward	CTACCCGCAGGAGCTGAACAA
	Reverse	AATCATGGACTGAAATGGTCTCCAG
hJNK	Forward	CAGGACTGCAGGAACGAGTT
	Reverse	CTCCCATGATGCACCCAACT
hP65	Forward	TGAACCGAAACTCTGGCAGCTG
	Reverse	CATCAGCTTGCGAAAAGGAGCC
hAp-1	Forward	GGATGTATGTCAGTGGACAGA
	Reverse	AAGCGCAGTATTTCCAGCACC
hMyD88	Forward	GTCTCCTCCACATCCTCCCT
	Reverse	CAGTTGCCGGATCTCCAAGT

2.12 Western blotting

Approximately 60 mg of lung tissue was homogenized in 500 μL radio immunoprecipitation assay (RIPA) lysis buffer and incubated on ice for 30 min with intermittent vortexing every 5 min. For cultured cells, proteins were extracted using ~60 μL RIPA lysis buffer per well. Equal protein amounts (40~60 μg) were separated by sodium dodecyl sulfate-polyacrylamide gel electrophoresis gels (6–12%) and transferred to polyvinylidene fluoride membranes (0.22 or 0.45 μm, selected based on target protein Mw). Membranes were blocked with 5% non-fat milk, then incubated overnight at 4 °C with primary antibodies, followed by HRP-conjugated secondary antibodies[32,38]. Protein bands were detected using Immobilon® Western Chemiluminescent HRP substrate and imaged with a W3000 system (Servicebio, Wuhan, China). Band intensities were quantified using Image–J software and normalized to housekeeping proteins (GAPDH, β-actin, or β-tubulin).

2.13 Data analysis

Statistical analysis was carried out using GraphPad Prism software, version 8.0 (San Diego, CA, USA). The data were initially analyzed for normality and homogeneity of variance using the Brown-Forsythe and Bartlett tests, respectively. Results were presented as the mean ± standard deviation (SD). The differences among groups were compared using one-way ANOVA followed by Tukey post hoc test, and the differences between two groups were performed using Student-*t*-test. Differences were considered to be significant at a $P < 0.05$.

3. Results

3.1 Purification and chemical analysis

After ÄKTA-FPLC separation, *A. japonicus*-derived carbohydrates were divided into 4 fractions, with AJ-2 exhibiting the highest yield (~32% of total carbohydrate, Figure 1A). AJ-2 was further purified via size exclusion chromatography, yielding the major fraction AJ-2I (~81% of AJ-2, Figure 1B), which displayed a symmetrical peak on HPGPC (Figure 1D). Its Mw was determined to be 135.8 kDa based on the standard curve (Figure 1C-D). Compositional analysis revealed that AJ-2I contained 57.6% carbohydrate, 27.0% sulfate, 13.0% uronic acid, and 2.4% protein. Monosaccharide analysis demonstrated that AJ-2I primarily consisted of mannose, GlcA, galacturonic acid (GalA), N-acetylgalactosamine (GalNAc), and fucose (Fuc) in a molar ratio of 4.3:1.5:2.0:1.0:18.6 (Figure 1E-F). GlcA and GalNAc took only approximately 5.3% and 3.5% of the total carbohydrates.

FT-IR spectrum of AJ-2I showed characteristic absorbance peaks of fucoidan (Figure 1G). The intense peak at 3428.04 cm^{-1} was assigned to the stretching vibration of hydroxyl groups (-OH). The great peak at 1056.07 cm^{-1} was attributed to the stretching vibrations of C–O–C and C–O–H groups. The obvious sulfate ester (O=S=O) peak was observed at 1252.34 cm^{-1}. The band at 848.60 cm^{-1} indicated that sulfate groups were predominantly located at the axial C2 positions and C4 positions[26,42]. Additionally, the weak peak at ~1748.40 cm^{-1} suggested the presence of esterified carboxyl groups[43].

3.2 Structural characteristics of A. japonicus-derived fucoidan AJ-2I

Given desulfation degrades the native structure of fucoidan[32,44], we performed methylation analysis directly on AJ-2I. The completeness of methylation was confirmed by the disappearance of O-H stretching vibrations (3428.04 cm^{-1}), and the significant increase in C-H stretching vibrations (2929.01 and 2870.11 cm^{-1}) in the FT-IR spectrum (Figure 1H). GC-MS analysis revealed that AJ-2I primarily consisted of [→2,3,4)-Fuc*p*-(1→], [→2,4)-Fuc*p*-(1→], [→3,4)-Fuc*p*-(1→], [→3)-Fuc*p*-(1→], [→4)-Fuc*p*-(1→], and [Fuc*p*-(1→] residues in a ratio of 15.9:6.4:7.7:8.5:1.0:1.3 (Figure 2A-B and Table 2). However, mannose and GalNAc residues were almost undetectable by GC-MS (Supplementary Figure 1A-C), suggesting the methylation process induced degradation of these residues, as reviewed by Hossain *et al*.[21].

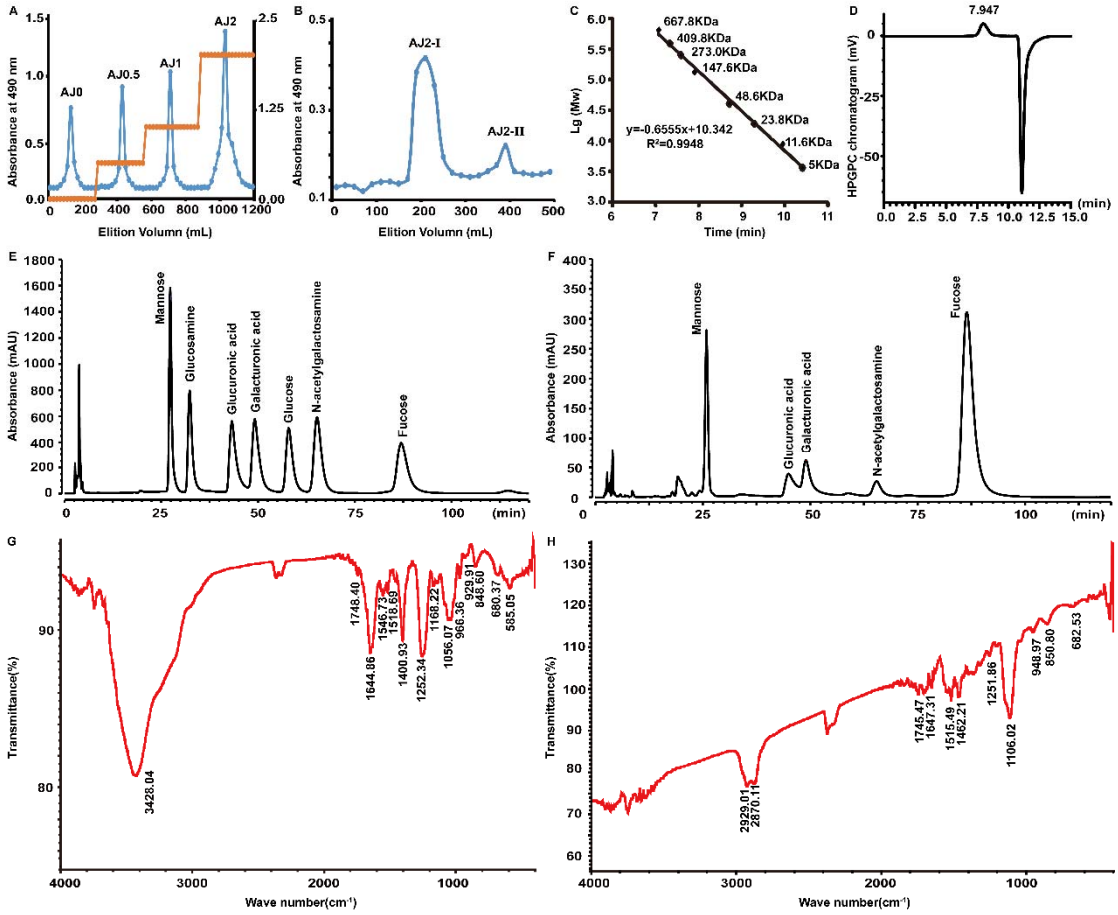

Figure 1. Purification and chemical analysis of *A. japonicus*-derived fucoidan AJ2-I. A, Stepwise fractionation of *A. japonicus*-derived carbohydrate on a Q-Sepharose™ Fast Flow column (50 × 300 mm) connected to an ÄKTA fast protein liquid chromatography (FPLC) system. B, Purification of the fraction AJ-2 via size-exclusion chromatography on a Sephacryl S200 HR column (2.6 × 90 mm). C, Standard curve made by dextran standards with different Mw. D, The purity and Mw of AJ-2I were analyzed by HPGPC using a TOSOH TSKgel G4000PWXL column with a RID-10A refractive index detector. E, Typical HPLC graph of seven mixed monosaccharide standards in an equal molar ratio after PMP pre-column derivatization. F, Monosaccharide composition of AJ-2I as revealed by HPLC after complete hydrolysis and PMP pre-column derivatization. G, FT-IR spectrum of AJ-2I. H, FT-IR spectrum of AJ-2I after complete methylation.

Table 2. The dominant partially methylated alditol acetates of fucoidan AJ-2I as revealed by GC-MS analysis.

Sugar derivatives	Linkage pattern	Ratio	Major mass fragments (m/z)
1,5-Ac$_2$-2,3,4-Me$_3$-Fuc*p*	Fuc*p* (1→	1.3	102.0, 115.0, 118.0, 131.0,162.0
1,4,5-Ac$_3$-2,3-Me$_2$-Fuc*p*	→4)Fuc*p* (1→	1.0	101.0, 118.0, 143.0, 161.0, 203.0, 247.0
1,3,5-Ac$_3$-2,4-Me$_2$-Fuc*p*	→3)Fuc*p* (1→	8.5	101.0, 118.0, 131.0, 160.0, 202.0, 234.0
1,3,4,5-Ac$_4$-2-Me-Fuc*p*	→3,4)Fuc*p* (1→	7.7	99.0, 118.0, 129.0, 173.0, 202.0, 275.0
1,2,4,5-Ac$_4$-3-Me-Fuc*p*	→2,4)Fuc*p* (1→	6.4	89.0, 128.0, 131.0, 202.0, 262.0
1,2,3,4,5-Ac$_5$-Fuc*p*	→2,3,4)Fuc*p* (1→	15.9	103.0, 115.0, 129.0, 146.0, 157.0, 303.0

^{1}H-NMR spectrum (Figure 2C) displayed characteristic proton signals ranging from δ 1.10 to 5.65 ppm. Typical H6 signals of Fuc*p* residues or methyl of *O*-acetyl (Ac) group appeared at δ 1.10-1.28 ppm, while *N*-Ac group resonance was dominated at δ 1.97 ppm[32,45,46]. A total of eighteen distinct anomeric proton signals (δ 5.65-4.40 ppm, labeled A-P) were determined in combination with 2D-NMR analysis (Figures 3A-B, Table 3). Glycosidic ring protons (H2~H5) primarily distributed in the δ 3.27-5.00 ppm region. The DEPT spectrum (Figure 2D) revealed characteristic anomeric carbon signals ranging from δ 94.82 to 104.25 ppm. The specific resonances for C6 of Fuc*p* or methyl of *O*-Ac were located at δ 15.37-15.62 ppm, the methyl signals of *N*-Ac presented at δ 22.56 ppm, and the methyl resonances of *O*-methyl appeared at δ 48.92

ppm[45-49]. The characteristic *N*-substituted carbon signal at δ 51.35 ppm further supported the present of *N*-linked sugars (Figure 2D)[45,46]. The inverted peak at δ 57.30 ppm in combination with correlations in ^{1}H-^{1}H COSY (1.10/3.57, Figure 3A) and HMQC spectra (3.57/57.30 and 1.10/15.13, Figure 3B), indicating the present of *O*-ethyl (Et) groups[47-50]. The carbonyl signals at δ 174.95 and 172.49 ppm were attributable to *N*-Ac and/or uronic acid carboxyl groups[32,49-51] The absence of inverted signals around 65 ppm, suggesting there were no C6 substituted sugar residues or sulfate groups in fucoidan AJ-2I[33,44,48].

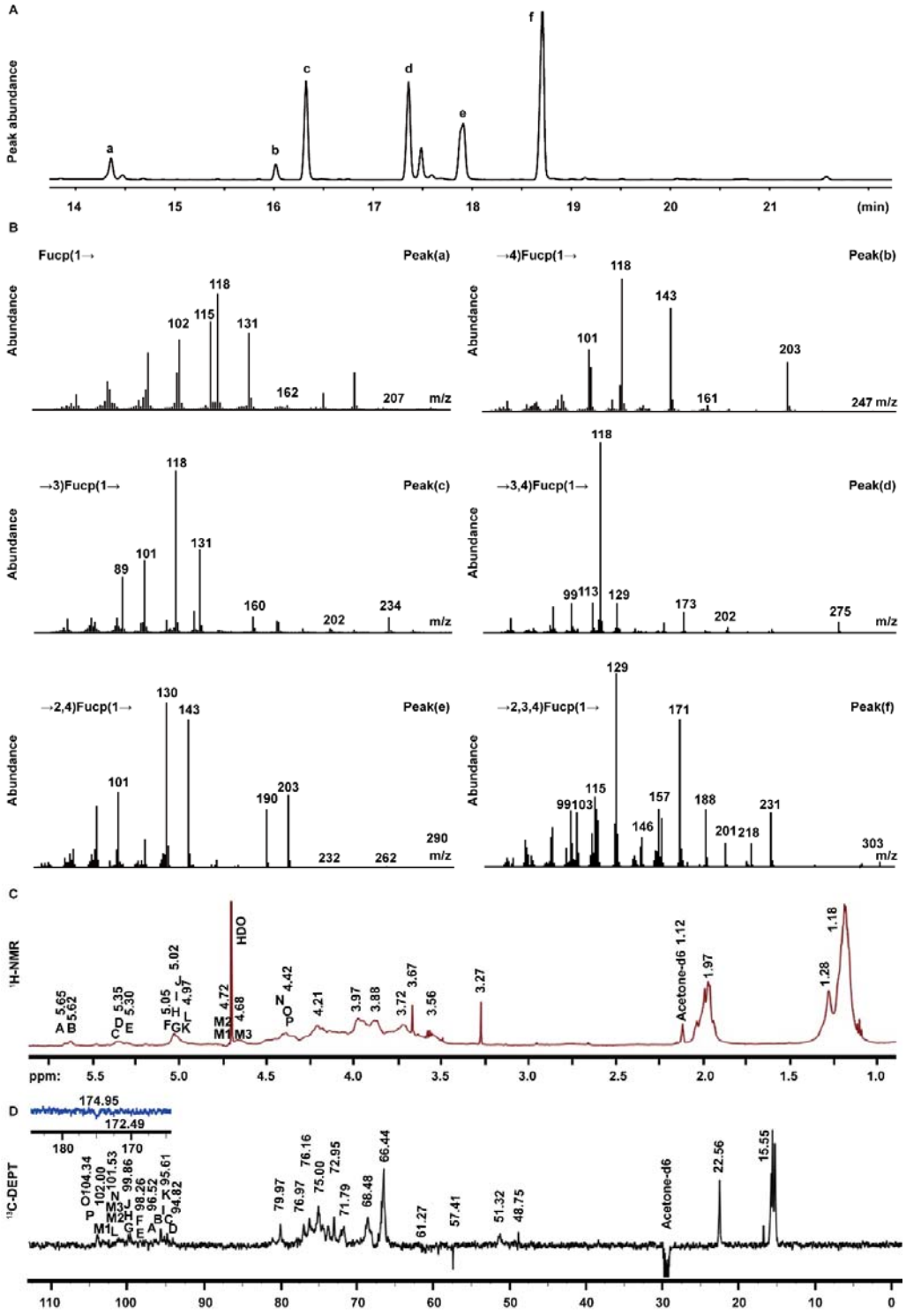

Figure 2. GC-MS analysis of partially methylated alditol acetates of AJ2-I and NMR analysis of AJ2-I. A, Total ion profile of the partially methylated alditol acetates. B, MS fragments and deduced sugar residues. C, ^{1}H-NMR spectrum. D, ^{13}C-DEPT spectrum.

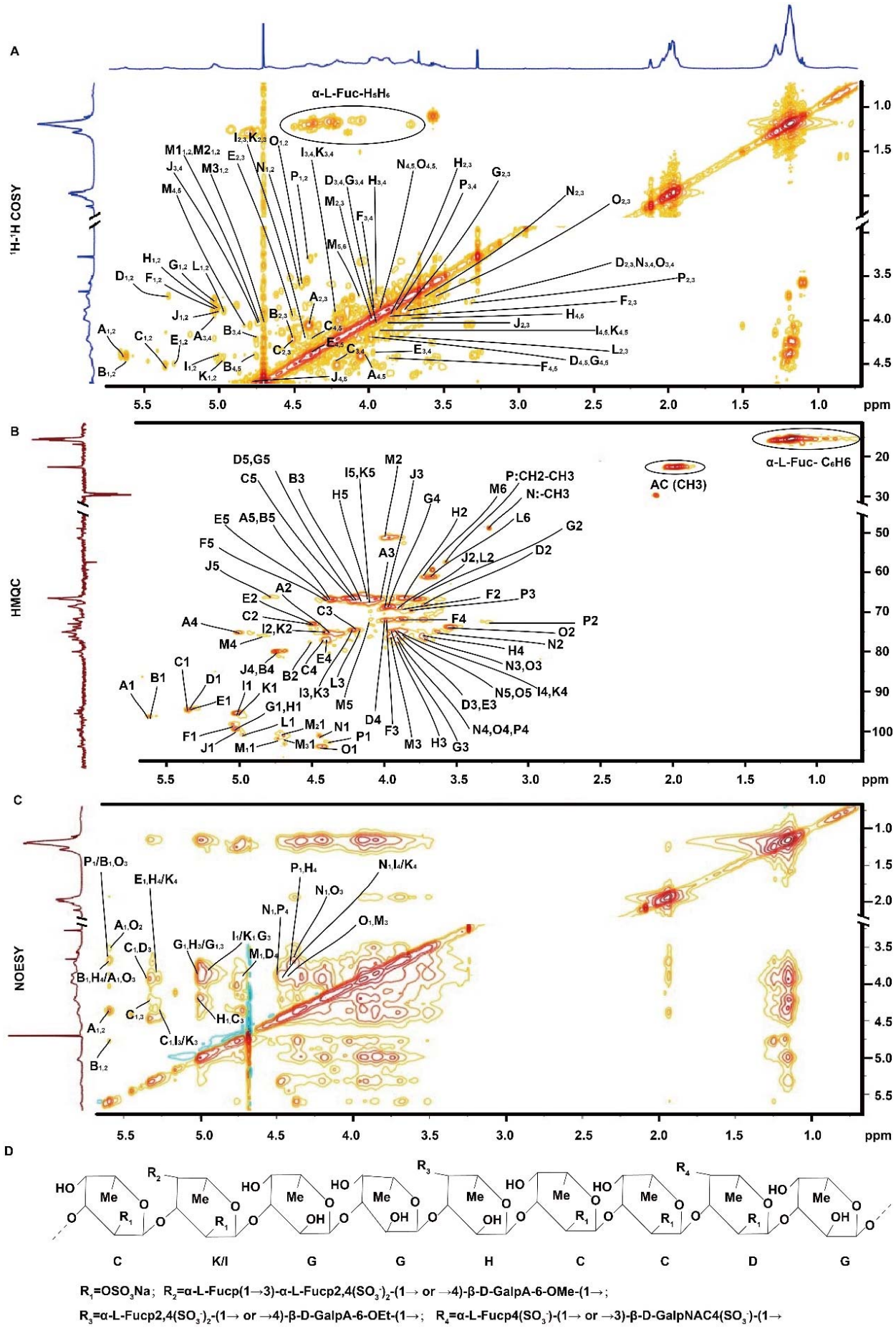

Figure 3. 2D-NMR analysis of AJ2-I. A, ^{1}H-^{1}H COSY spectrum. B, HMQC spectrum. C, NOESY spectrum. D, The deduced structure of AJ2-I.

Table 3. NMR chemical signal assignment for AJ2-I.

Residue	H1/C1	H2/C2	H3/C3	H4/C4	H5/C5	H6/C6	*N*-C=O	-CH_2-	-CH_3
A	5.65	4.39	4.00	5.02	4.38	1.18			
α-L-Fuc*p*2,4(SO_3^-)$_2$-(1→	96.52	75.30	66.87	75.26	66.64	15.37			
B	5.62	4.49	4.18	4.75	4.38	1.18			
α-L-Fuc*p*2,4(SO_3^-)$_2$-(1→	96.52	77.94	67.80	81.19	66.64	15.37			
C	5.37	4.51	4.22	4.40	4.44	1.18			
→3)-α-L-Fuc*p*2,4(SO_3^-)$_2$-(1→	94.82	73.09	74.46	77.08	66.62	15.62			
D	5.35	3.73	3.91	3.98	4.20	1.18			
→3,4)-α-L-Fuc*p*-(1→	94.82	68.3	75.26	72.14	66.72	15.62			
E	5.30	4.49	3.94	4.39	4.38	1.18			
→3)-α-L-Fuc*p*2,4(SO_3^-)$_2$-(1→	94.62	73.09	75.02	77.20	66.67	15. 62			
F	5.05	3.86	3.96	3.87	4.43	1.18			
α-L-Fuc*p*(1→	98.54	69.07	71.96	72.09	67.09	15.62			
G	5.02	3.78	3.90	3.98	4.20	1.18			
→3)-α-L-Fuc*p* (1→	99.86	66.91	77.93	68.69	66.72	15.62			
H	5.02	3.86	3.94	3.73	4.10	1.18			
→3,4)-α-L-Fuc*p* (1→	99.86	66.95	74.99	76.77	66.68	15.62			
I	5.02	4.42	4.21	3.93	4.08	1.15			
→3,4)-α-L-Fuc*p*2(SO_3^-)-(1→	95.61	75.33	74.55	75.13	66.99	15.62			
J	5.01	3.88	4.02	4.74	4.78	1.28			
α-L-Fuc*p*4(SO_3^-)-(1→	99.94	68.99	68.86	80.02	66.28	15.62			
K	4.99	4.42	4.21	3.93	4.08	1.15			
→3,4)-α-L-Fuc*p*2(SO_3^-)-(1→	95.61	75.33	74.55	75.13	66.99	15.62			
L	4.97	3.89	4.18	/	/	3.66			
→3)-α-D-Man-(1→	100.91	68.95	74.79	/	/	61.16			
M1	4.72	3.96	3.95	4.84	4.06	3.72			1.97
→3)-β-D-Gal*p*NAC4(SO_3^-)-(1→	102.00	51.35	76.48	76.06	73.25	61.16	174.95		22.56
M2	4.71	3.96	3.95	4.84	4.06	3.72			1.97
→3)-β-D-Gal*p*NAC4(SO_3^-)-(1→	100.63	51.35	76.48	76.06	73.25	61.16	174.95		22.56
M3	4.68	3.96	3.95	4.84	4.06	3.72			1.97
→3)-β-D-Gal*p*NAC4(SO_3^-)-(1→	101.53	51.35	76.48	76.06	73.25	61.16	174.95		22.56
N	4.45	3.61	3.72	3.91	3.86				3.27
→4)-β-D-Gal*p*A-6-OMe-(1→	101.34	75.10	76.86	76.30	76.51	172.49			48.92
O	4.42	3.55	3.70	3.91	3.86				
→3,4)-β-D-Glc*p*A(1→	104.34	74.00	77.20	76.30	76.51	174.95			
P	4.40	3.31	3.81	3.92	/			3.57	1.10
→4)-β-D-Gal*p*A-6-OEt-(1→	103.1	72.59	69.76	77.83	/	172.79		57.30	15.13

H1-H3 and H5-H6 correlations of carbohydrates are generally identifiable through ^{1}H-^{1}H COSY spectrum. For Fuc*p* units (Table 3), we identified α-L-Fuc*p*(1→, →3)-α-L-Fuc*p*(1→, α-L-Fuc*p*4(SO3-)-(1→, →3,4)-α-L-Fuc*p*-(1→, α-L-Fuc*p*2,4(SO3-)$_2$-(1→, and →3,4)-α-L-Fuc*p*2(SO3-)-(1→ and →3)-α-L-Fuc*p*2,4(SO3-)$_2$-(1→ residues, which corresponding to [Fuc*p*-(1→], [→3)-Fuc*p*-(1→], [→4)-Fuc*p*-(1→], [→3,4)-Fuc*p*-(1→], [→2,4)-Fuc*p*-(1→], and [→2,3,4)-Fuc*p*-(1→] fucosyl residues, respectively, as revealed by the methylation analysis (Table 2). These NMR data demonstrated that Fuc*p*

residues were mainly consisted of [→3)-Fuc*p*-(1→] residues with branching at C4 positions. Sulfation at C2 positions of Fuc*p* residues was characterized by the down-field shifts of these resonances (e.g., δ 4.51/73.09, 4.42/75.33) compared to unsubstituted counterparts (δ 66.5-71.5/3.7-4.1 ppm). Furthermore, C4 sulfation signals were generally observed at δ 3.9-5.0/72-82 ppm compared to δ 3.9-4.2/68.5-70.5 ppm for non-sulfated residues[32,42,46,52,53]. These characteristic chemical shifts are reliable markers for identifying sulfate substitution positions. As exemplified by residue A, we observed sequential correlations of H1→H6 (δ 5.65→4.39→4.00→5.02→4.38→1.18) by the ^{1}H-^{1}H COSY and NOESY spectra (Figures 3A and 3C). HMQC analysis (Figure 3B) confirmed these assignments through carbon-proton correlations: H1/C1 (δ 5.65/96.52), H2/C2 (δ 4.39/75.30), H3/C3 (δ 4.00/66.87), H4/C4 (δ 5.02/75.26), H5/C5 (δ 4.38/66.64), and H6/C6 (δ 1.18/15.37). These data collectively identified residue A as α-L-Fuc*p*2,4(SO3-)$_2$-(1→ due to the significant down-field shifts of H2/C2 and H4/C4 signals. The Fuc*p* residues without sulfation were also identified. For instance, residue G showed H1→H6 correlations (5.02→3.78→3.90→3.98→4.20→1.18) in the ^{1}H-^{1}H COSY spectrum (Figure 3A) and exhibited C1→C6 signals (Table 3) in the HMQC spectrum (Figure 3B). This residue was assigned as [→3)-Fuc*p*-(1→] glycosyl based on the above information and the literatures[54-56].

Moreover, →3)-β-D-Gal*p*NAC4(SO_3^-)-(1→, →4)-β-D-Gal*p*A-6-OMe-(1→, →4)-β-D-Gal*p*A-6-O-Et-(1→, →3,4)-β-D-Glc*p*A-(1→, and →2)-α-D-Man*p*-(1→ residues were also identified through 2D-NMR analysis. For instance, the correlations of residue M1, including H1→H6 (δ 4.72→3.96→3.95→4.84→4.06→3.72) and C1→C6 (δ 102.00→51.35→76.48→76.06→73.25→61.16 ppm) were assigned based on the ^{1}H-^{1}H COSY and HMQC spectra and summarized in Table 3. The significant high-field shift of C2 (δ 51.35 ppm) suggested that this carbon was *N*-substituted with Ac as aforementioned. This result was consistent with the presence of carbonyl group at δ 174.95 ppm and methyl signals of Ac (1.97/22.56, Figure 3B). We observed correlation signals between H6 of residue M1 and CH_3 of *N*-Ac (3.72/1.97) in the NOESY spectrum (Figure 3C), further confirming the presence of *N*-Ac in this residue. Additionally, the significant down-field shift of H4/C4 (4.84/76.06) demonstrated that residue M was sulfated at C4 position[46,57]. Similarly, the residues M2 and M3 were attributed to →3)-β-D-Gal*p*NAC4(SO_3^-)-(1→ glycosyls. For residue N, the H1/C1 (4.45/101.34), H2/C2 (3.61/75.10), H3/C3 (3.72/76.86), H4/C4 (3.91/76.30), and H5/C5 (3.86/76.51) were assigned through 2D-NMR spectra. This sugar residue was determined as →4)-β-D-Gal*p*A-6-OMe-(1→ glycosyl based on the presence of *O*-methyl signals (3.27/48.92) and carboxyl signal at 172.49 ppm (Figure 2D and Figure 3B) and the corresponding literatures[47-50]. Similarly, the residue P was assigned as →4)-β-D-Gal*p*A-6-O-Et-(1→ due to the presence of *O*-Et signals (3.57/57.30-1.10/15.13) and the correlations in 2D-NMR spectra (Figure 3A-C). Furthermore, the residue O was assigned as →3,4)-β-D-Glc*p*A-(1→ residue based on the literatures[44,46,58]. Additionally, the residue L was attributed to →3)-α-D-Man*p*-(1→ glycosyl due to the down-field shifts of H3/C3 (4.18/74.79) based on the correlations in the 2D-NMR spectra and references[52,58,59].

NOESY and HMBC experiments were further applied to clarify the structure of AJ2-I. However, HMBC spectrum (Supplementary material 1) only showed useful correlations between C**H**$_3$ and **C**H$_2$ of *O*-Et (1.10/57.30) and C**H**$_3$ and C5 of Fuc*p* residues (1.18/66.67) after extended acquisition (16 h), greatly limiting sequence determination. Notably, the NOESY spectrum revealed key inter-glycosidic correlations (Figure 3C). For instance, correlations were observed between H1 of residue C (δ 5.37) and H3 of residue I/K (δ 4.21), between H1 of residue I/K (δ 5.02,4.99) and H3 of residue G (δ 3.90), between H1 of residue G (δ 5.02) and H3 of residue G and H (δ 3.90,3.94). Furthermore, correlations between H1 of residue F (δ 5.05) and H3 of residue E (δ 3.94) and between H1 of residue E with H4 of residue K/I (δ 3.93) suggested the presence of α-L-Fuc*p* (1→3)-α-L-Fuc*p*2,4(SO3-)$_2$-(1→ residues linked to the C4 position of reside H. Additional potential side chains were also assigned base on NOESY correlations. We also observed a correlation between H1 of residue O (δ 4.42) and H3 of residue M (δ 3.95), indicating the presence of →4)-β-D-Glc*p*A-(1→3)-β-D-Gal*p*NAC4(SO_3^-)-(1→ residues. Correlations between H1 of residue A/B (δ 5.65,5.62) and H4 of residue H (δ 3.73) suggested that residues A/B were linked to the C4 positions of →3,4)-α-L-Fuc*p*(1→ glycosyl units. Additionally, H1 of residue M was correlated with H4 of residue D, H1 or residue N was correlated with H4 or residue I/K, and H1 of residue O/P was correlated with H4 of residue H, suggesting the residues M, N, O, and P, may also linked to the C-4 positions of the →3,4)-α-L-Fuc*p*(1→ glycosyls. These correlations collectively support the backbone structure of AJ2-I as depicted in Figure 3D.

3.3 Fucoidan AJ2-I attenuated ALI in LPS-challenged C57BL/6J mice

H & E staining images clearly revealed that LPS induced ALI, as demonstrated by significant increase in alveolar wall thickness (~97.6%) and cell infiltration (1.9-fold) compared to the BC group ($P < 0.0001$, Figures 4A-C). These pathological changes were ameliorated by treatment with Dex and AJ2-I (Figures 4A-C). Specifically, the F-L and F-H groups significantly attenuated cell infiltration by 19.7% ($P < 0.05$) and 42.2% ($P < 0.0001$), respectively, and decreased alveolar wall thickness by approximately 27.4% ($P < 0.01$) and 42.4% ($P < 0.0001$), respectively. Compared to the BC group, lung tissue AST and ALT levels in the Mod group were elevated by approximately 1.8-fold ($P < 0.01$) and 1.7-fold ($P < 0.05$), respectively. These increases were significantly mitigated by Dex and AJ2-I intervention ($P < 0.05$, Figures 4D-E). Similarly, the Mod group significantly increased plasma levels of AST and ALT by 1.9-fold and 2.1-fold, respectively, compared to the BC group ($P < 0.05$), whereas treatment groups exhibited significant reductions in these markers to varying degrees ($P < 0.05$, Figures 4F-G).

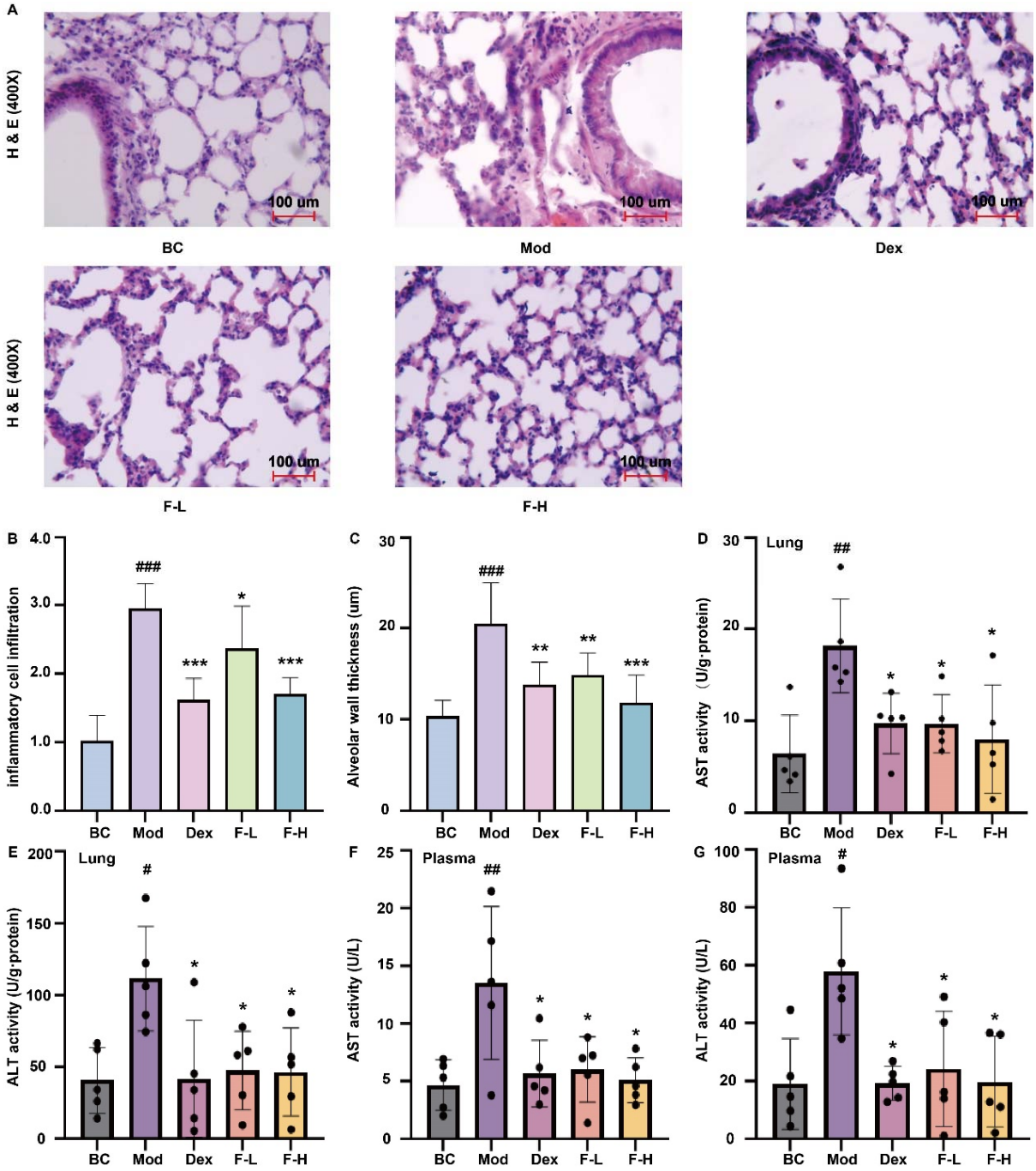

Figure 4. Typical H & E staining images, and effects of AJ2-I on the ALT and AST activity in LPS-challenged C57BL/6J mice (n=5). A, Typical H & E staining images of mice lung after drug intervention and LPS challenge (magnification: 400 ×). B, Alterations in inflammatory cell infiltration of the lung tissues. C, Alterations in alveolar wall thickness of the lung tissues. D and E, AST and ALT activity of the lung tissues, respectively. F and G, Plasma AST and ALT activity, respectively. BC: blank control; Mod: model, the mice were treated with LPS (5.0 mg/kg); Dex: dexamethasone, the mice were first treated with Dex (10 mg/kg) prior to LPS (5.0 mg/kg) challenge; F-L: the mice were first treated with low-dosage AJ-2I (50 mg/kg) prior to LPS (5.0 mg/kg) challenge; F-H: the mice were first treated with high-dosage AJ-2I (200 mg/kg) prior to LPS (5.0 mg/kg) challenge. $^{\#}P < 0.05$ *vs*. BC group; $^{\#\#}P < 0.01$ *vs*. BC group; $^{\#\#\#}P < 0.001$ *vs*. BC group; $^{*}P < 0.05$ *vs*. Mod group; $^{**}P < 0.01$ *vs*. Mod group; $^{***}P < 0.001$ *vs*. Mod group. All the abbreviations are applicable for the subsequent figures 5-6 and the statistical symbols are suitable for the following figures 5-9.

3.4 Fucoidan AJ2-I inhibited expression of pro-inflammatory factors and TLR2/4-MyD88 signaling in the mice lung

Compared to the BC group, the Mod group significantly elevated the expression of IL-6, IL-1β, and TNF-α by approximately 2.5-fold ($P < 0.01$), 3.3-fold ($P < 0.05$), and 2.0-fold ($P < 0.01$), respectively

(Figures 5A-C). The fucoidan treatment dose-dependently suppressed these inflammatory markers. The F-H group showed the most pronounced effects, reducing IL-6 (89.8%, $P < 0.001$), IL-1β (88.7%, $P < 0.01$), and TNF-α (84.6%, $P < 0.001$) compared to the Mode group. Notably, the F-H group outperformed Dex in suppressing IL-6 (78.3% reduction) and TNF-α (70.3% reduction) ($P < 0.05$, Figures 5A and 5C). Consistent with mRNA findings, protein levels of these cytokines were significantly elevated in the Mod group versus the BC group (Figures 5D-F). Fucoidan intervention dose-dependently attenuated these increases, with the F-H group reducing IL-6 (66.2%), IL-1β (59.2%), and TNF-α (54.5%) compared to the Mod group ($P < 0.05$, Figures 5D-F).

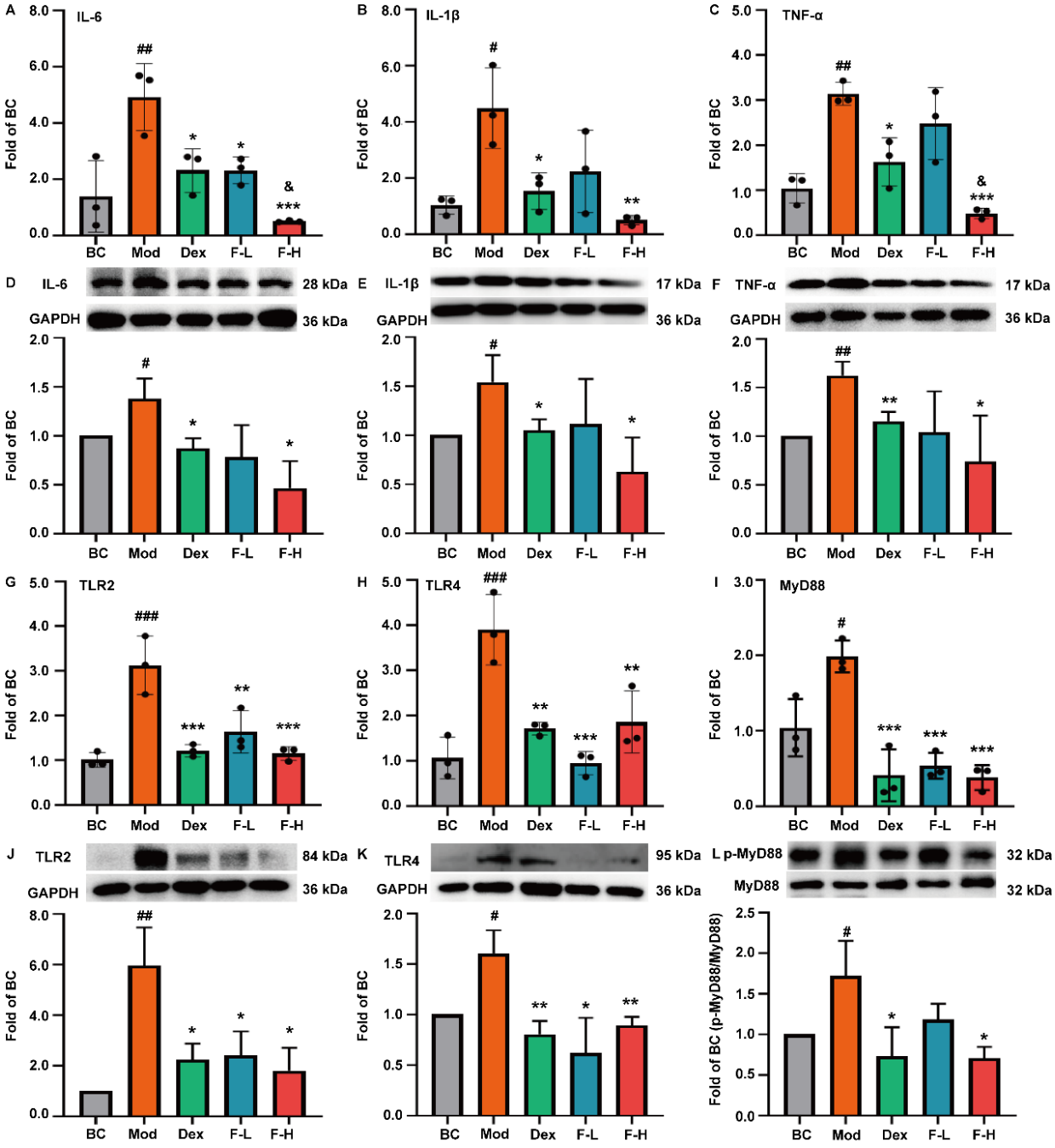

Figure 5. Effects of AJ2-I on the expression of pro-inflammatory cytokines and TLR2/4 signaling in the lung tissues (n=3). The mRNA expression of A, IL-6; B, IL-1β; and C, TNF-α. The levels of D, IL-6; E, IL-1β; and F, TNF-α. The mRNA expression of G, TLR2; H, TLR4; and I, MyD88. The levels of J, TLR2; K, TLR4; and L, p-MyD88. $^{\&}P < 0.05$ *vs*. Dex group.

As expected, LPS challenge significantly upregulated the expression of TLR2, TLR4, and MyD88 by 2.1-fold ($P < 0.001$), 2.7-fold ($P < 0.001$), and 90.5% ($P < 0.05$), respectively, compared to the BC group (Figures G-I). Dex intervention effectively suppressed these increases compared to the Mod group ($P < 0.01$ or 0.001, Figures 5G-I). Similarly, fucoidan intervention dose-dependently attenuated these gene expression, with reductions exceeding 47.6% (TLR2, $P < 0.01$), 52.1% (TLR4, $P < 0.01$), and 72.9% (MyD88, $P < 0.001$). Western blotting demonstrated that the Mod group exhibited elevated levels of TLR2 (4.9-fold, $P < 0.01$), TLR4 (1.7-fold, $P < 0.05$), and p-MyD88 (72.1%, $P < 0.05$) proteins compared to the BC group (Figures 5J-L). Notably, the F-H group demonstrated comparable efficacy as that of Dex, decreasing TLR2, TLR4, and p-MyD88 by 69.7% ($P < 0.05$), 80.4% ($P < 0.01$), and 58.9% ($P < 0.05$), respectively, compared to the Mod group (Figures 5J-L).

3.5 Fucoidan AJ2-I suppressed the PI3K/AKT and MAPK signaling pathways in the mice lung

Compared to the BC group, the Mod group exhibited significantly increased expression of PI3K (1.9-fold, $P < 0.05$) and AKT (3.4-fold, $P < 0.001$) (Figures 6A-B). Treatment with Dex reduced these levels by 56.9% (PI3K) and 38.9% (AKT) ($P < 0.05$), while the F-H group showed more pronounced suppression (67.3% for PI3K, $P < 0.05$; 79.9% for AKT, $P < 0.001$), with significantly greater inhibition of AKT than Dex ($P < 0.05$, Figure 6B). At the protein level, LPS significantly upregulated p-PI3K (43.9%, $P < 0.001$) and p-AKT (89.7%, $P < 0.01$) (Figures 6E-F). Both Dex and F-H groups attenuated these increases, with F-H group demonstrating superior efficacy. Moreover, the Mod group exhibited significantly elevated expression of ERK (1.5-fold, $P < 0.05$, Figure 6C) and JNK (2.1-fold, $P < 0.01$, Figure 6I) compared to the BC group. Dex treatment effectively reduced these increases by 75.4% for ERK and 80.3% for JNK ($P < 0.01$), while fucoidan intervention groups showed dose-dependent reductions (>59.4% for ERK and >66.5% for JNK, $P < 0.05$ or 0.01, Figures 6C and 6I). However, P38 gene expression was undetectable (Ct > 30, Figure 6D). At the protein level, LPS challenge significantly increased phosphorylation levels of ERK (3.6-fold, $P < 0.01$, Figure 6G), P38 (53.5%, $P < 0.01$, Figure 6H), and JNK (64.8%, $P < 0.001$, Figure 6L). Both Dex and F-H treatments markedly attenuated phosphorylation of these proteins. F-H significantly reduced p-ERK, p-P38, and p-JNK by 66.8%, 34.9%, and 42.6%, respectively, compared to the Mod group ($P < 0.05$).

LPS stimulation significantly upregulated the expression of P65-NF-κB (1.2-fold) ($P < 0.01$, Figures 6J) and AP-1 (2.6-fold) compared to the BC group ($P < 0.01$, Figures 6K). AJ2-I intervention groups demonstrated dose-dependent suppression of these transcriptional factors, with the F-H group showing particularly strong inhibition (79.8% reduction for P65-NF-κB and 88.6% for AP-1, $P < 0.001$ versus Mod group). Notably, the F-H group's effect on AP-1 expression exceeded that of Dex by 77.9% ($P < 0.05$, Figure 6K). LPS significantly enhanced the phosphorylation levels of P65 (2.7-fold) and AP-1 (21.9%) proteins ($P < 0.01$, Figures 6M-N). Dex treatment attenuated these phosphorylation levels ($P < 0.05$), while fucoidan showed superior dose-dependent effects. The F-H group achieved remarkable reductions of 81.7% (p-P65, $P < 0.01$, Figure 6M) and 81.5% (p-AP-1, $P < 0.001$, Figure 6N) compared to the Mod group, and outperformed Dex by further reducing p-P65 (67.2%, $P < 0.01$) and p-AP-1 (69.6%, $P < 0.05$) levels.

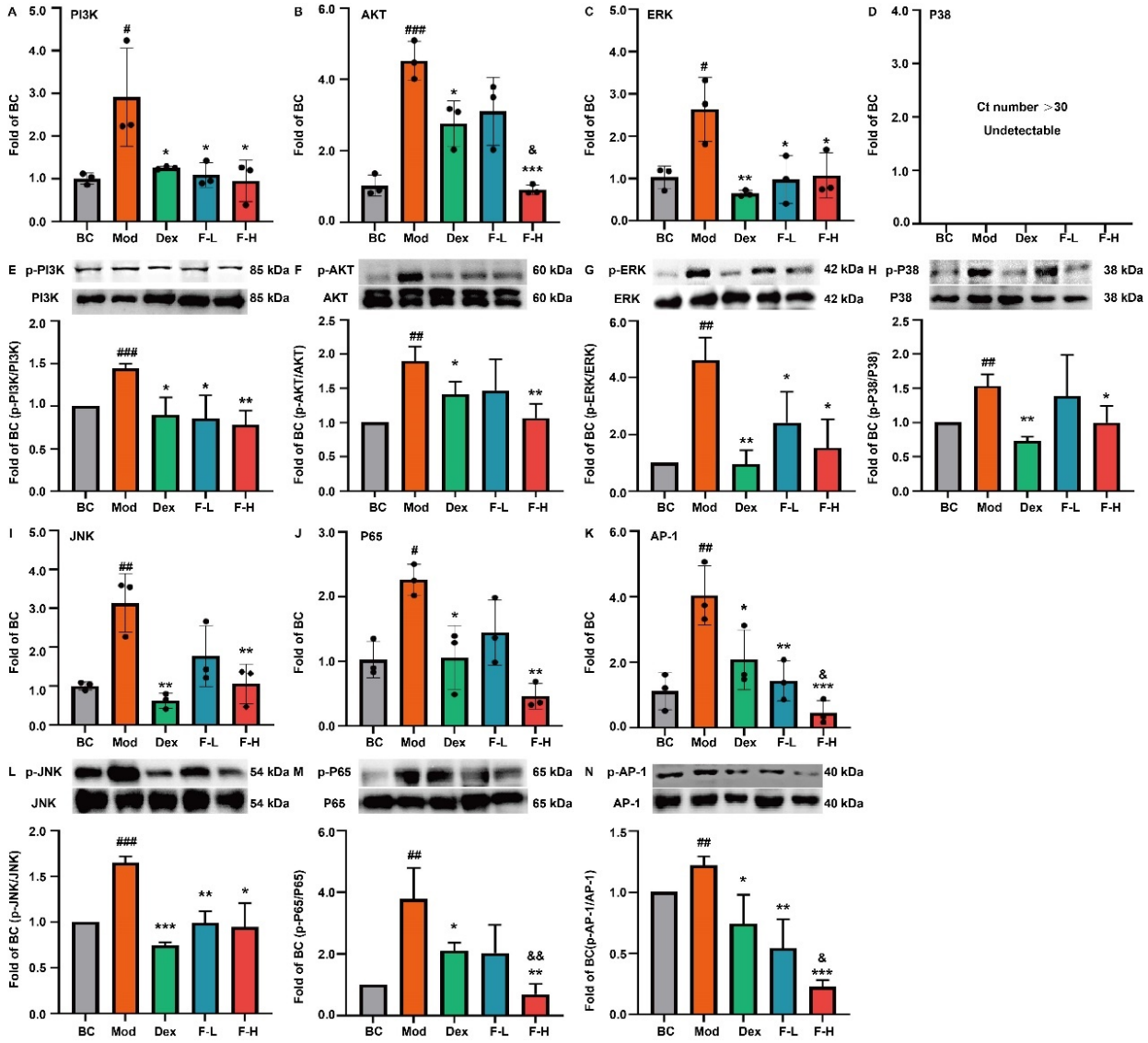

Figure 6. Effects of AJ2-I on the PI3K-AKT and MPAK-NF-κB/AP-1 signaling in the lung tissues (n=3). The mRNA expression of A, PI3K; B, AKT; C, ERK; and D, p38-MAPK. The phosphorylation levels of E, PI3K; F, AKT; G, ERK; and H, p38-MAPK. The mRNA expression of I, JNK; J, p65-NF-κB; and K, AP-1. The phosphorylation levels of L, JNK; M, p65-NF-κB; and N, AP-1. $^{\&}P < 0.05$ *vs*. Dex group; $^{\&\&}P < 0.01$ *vs*. Dex group.

3.6 Fucoidan AJ2-I reduced expression of pro-inflammatory factors and TLR2/4-MyD88 signaling in LPS-challenged A549 cells

Both the MTT and LDH release assays demonstrated that AJ2-I exhibited low cytotoxicity and minimal impact on cell membrane integrity in both A549 cells and HUVECs at concentrations up to 40 μg/mL (Figures 7A-D). In A549 cells, LPS challenge significantly upregulated the expression of IL-6, IL-1β, and TNF-α by 66.6% ($P < 0.05$), 1.7-fold ($P < 0.01$), and 3.0-fold ($P < 0.01$), respectively, compared to the BC group (Figures 7E-G). Treatment with Dex and AJ2-I significantly reduced expression of these cytokines. The F-H group demonstrated particularly strong inhibition, reducing IL-6 (87.1%), IL-1β (90.6%), and TNF-α (84.0%) expression ($P < 0.001$), with superior efficacy compared to Dex ($P < 0.05$, Figures 7 E-G). These mRNA findings were mirrored at the protein level, where LPS increased IL-6 (59.8%, $P < 0.01$), IL-1β (47.7%, $P < 0.01$), and TNF-α (98.3%, $P < 0.05$) protein levels versus the BC group (Figures 7H-J). Dex treatment reduced these proteins by 35.8% (IL-6), 39.6% (IL-1β), and 40.6% (TNF-α) ($P < 0.05$), while

fucoidan interventions showed dose-dependent effects, with the F-H group achieving reductions of 77.8% (IL-6, $P < 0.01$), 69.2% (IL-1β, $P < 0.001$), and 64.5% (TNF-α, $P < 0.01$). Notably, the F-H group's effects on IL-6 and IL-1β proteins exceeded Dex by 65.4% and 48.9%, respectively ($P < 0.05$, Figures 7H-I).

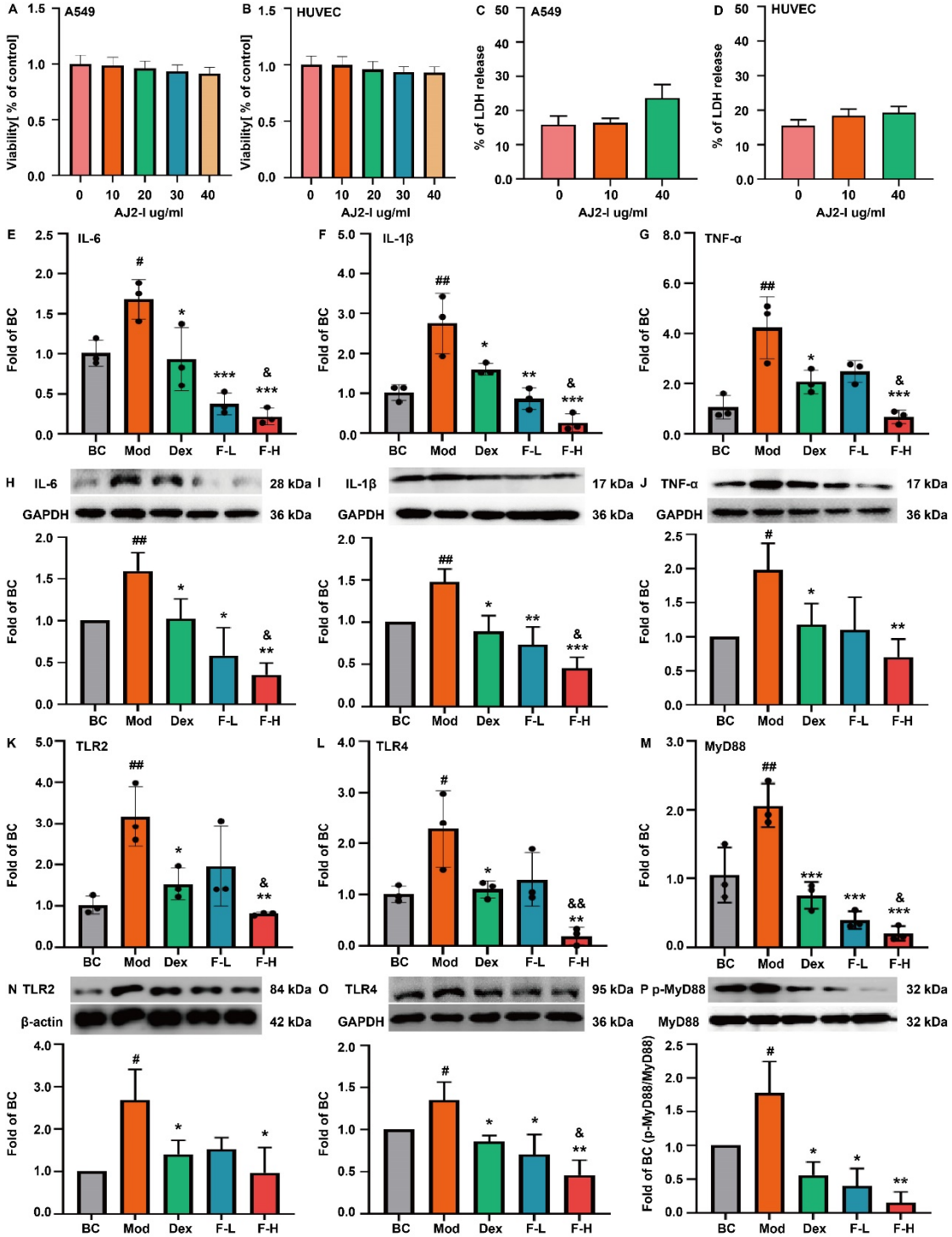

Figure 7. Safety evaluation and effects of AJ2-I on pro-inflammatory cytokine expression and TLR2/4 signaling in A549 cells (n=3). A and B, Viability of A549 cells (A) and human umbilical vein endothelial cells (HUVECs) (B) following 24 h treatment with increasing concentrations of AJ2-I (0-40 μg/mL). C and D, Lactate dehydrogenase (LDH) release from A549 cells (C) and HUVECs (D) after 24 h intervention with AJ2-I (0, 10, 40 μg/mL). The mRNA expression of E, IL-6; F, IL-1β; and G, TNF-α. The levels of H, IL-6; I, IL-1β; and J, TNF-α. The mRNA expression of K, TLR2; L, TLR4; and M, MyD88. The levels of N, TLR2; O, TLR4; and P, p-MyD88. BC: blank control; Model: A549 cells were treated with LPS (1.0 μg/mL); Dex: dexamethasone, cells were pre-treated with Dex (1.0 μM) prior to LPS (1.0 μg/mL) challenge; F-L: cells were pre-treated with AJ-2I (10 μg/mL) prior to LPS (1.0 μg/mL) challenge; F-H: cells were pre-treated with AJ-2I (40 μg/mL) prior to LPS (1.0 μg/mL) challenge. All the abbreviations are applicable for the subsequent figures 8-9. $^{\&}P < 0.05$ *vs*. Dex group; $^{\&\&}P < 0.01$ *vs*. Dex group.

As expected, LPS stimulation significantly upregulated the expression of TLR2 (2.1-fold) ($P < 0.01$), TLR4 (1.3-fold) ($P < 0.05$), and MyD88 (96.9%) ($P < 0.01$) compared to the BC group ($P < 0.05$ or 0.01, Figures 7K-M). Fucoidan interventions dose-dependently suppressed these genes, with the F-H group showing particularly strong inhibition (TLR2: 74.5%; TLR4: 91.6%; MyD88: 90.0%; $P < 0.01$ or 0.001 versus Mod group) and superior efficacy to Dex ($P < 0.05$ or $P < 0.01$). Western blot analysis confirmed these findings, revealing LPS-induced increases in TLR2 (1.7-fold), TLR4 (35.2%), and p-MyD88 (77.3%) proteins ($P < 0.05$, Figures 7N-P). Dex treatment reduced the levels of these proteins by 47.8% (TLR2), 36.5% (TLR4), and 68.7% (p-MyD88) ($P < 0.05$), while the F-H group demonstrated more potent effects, with its TLR4 suppression exceeding Dex by 46.7% ($P < 0.05$, Figure 7O).

3.7 Fucoidan AJ2-I suppressed the PI3K/AKT and MAPK signaling pathways in LPS-challenged A549 cells

LPS challenge significantly upregulated PI3K (1.7-fold, $P < 0.01$) and AKT (49.3%, $P < 0.05$) expression compared to the BC group (Figures 8A-B). Dex treatment effectively reduced these increases by 54.2% (PI3K, $P < 0.05$) and 72.4% (AKT, $P < 0.001$), with AJ2-I showing comparable efficacy to Dex. At the protein level, LPS elevated p-PI3K (35.4%, $P < 0.05$) and p-AKT (90.4%, $P < 0.01$) levels (Figures 8E-F), which were significantly suppressed by all treatments. Notably, the F-H group showed superior inhibition of p-PI3K (43.8% greater reduction than Dex, $P < 0.01$, Figure 8E). Similarly, LPS increased ERK (85.4%) and JNK (2.3-fold) expression ($P < 0.01$, Figures 8C, 8I), while Dex and AJ2-I significantly decreased these increases. However, p38 mRNA remained undetectable (Figure 8D). LPS significantly enhanced phosphorylation of ERK (50.8%, $P < 0.001$), P38 (80.8%, $P < 0.001$), and JNK (67.5%, $P < 0.01$) (Figures 8G-H, 8L), while both Dex and F-H treatments similarly reduced these phosphorylation events by approximately 50% ($P < 0.01$ or 0.001).

Consistently, LPS challenge significantly upregulated the expression of P65-NF-κB (1.7-fold) and AP-1 (1.8-fold) compared to the BC group ($P < 0.05$, Figures 8J-K). Dex treatment effectively reduced these increases by 60.2% (P65-NF-κB) and 55.7% (AP-1) versus the Mod group, while fucoidan interventions showed dose-dependent suppression, with the F-H group achieving reductions of 60.1% (P65-NF-κB, $P < 0.05$) and 86.5% (AP-1, $P < 0.01$). Notably, the F-H group demonstrated superior efficacy to Dex in suppressing AP-1 expression ($P < 0.05$, Figure 8K). At the protein level, both Dex and F-H treatments significantly attenuated phosphorylation events: they decreased p-P65 by 64.5% and 67.1% ($P < 0.01$, Figure 8M), respectively, and lowered p-AP-1 levels by 32.6% ($P < 0.05$) and 60.4% ($P < 0.01$), respectively (Figure 8N), compared to the Mod group.

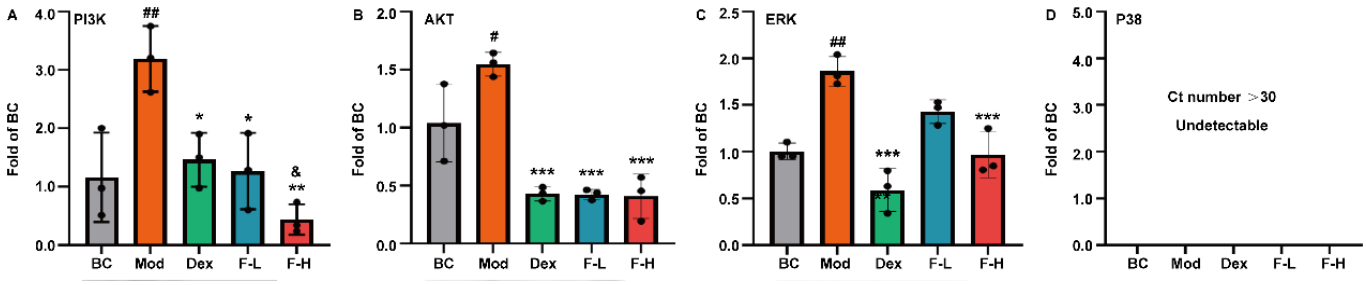

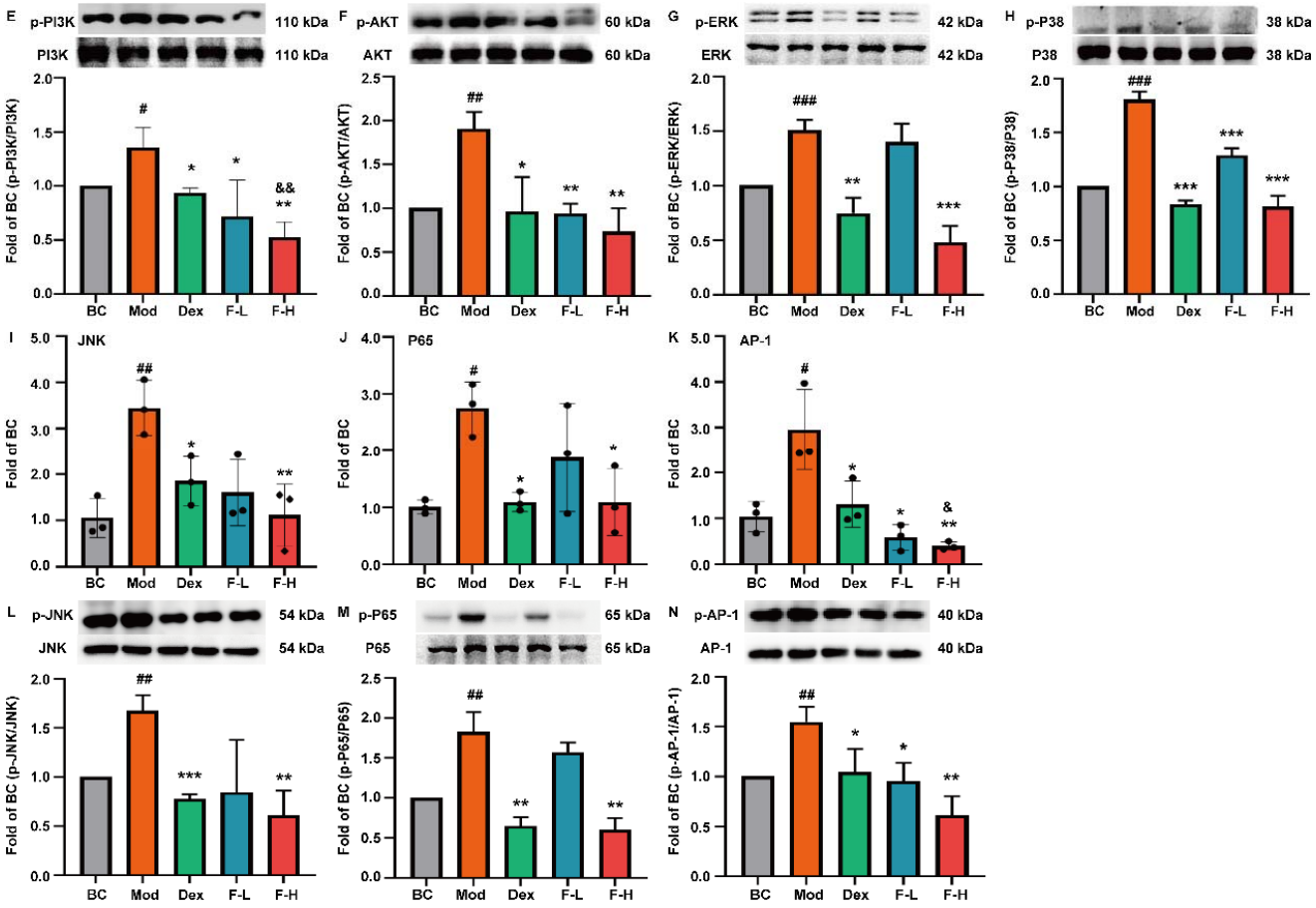

Figure 8. Effects of AJ2-I on the PI3K-AKT and MPAK-NF-κB/AP-1 signaling in A549 cells (n=3). The mRNA expression of A, PI3K; B, AKT; C, ERK; and D, p38-MAPK. The phosphorylation levels of E, PI3K; F, AKT; G, ERK; and H, p38-MAPK. The mRNA expression of I, JNK; J, p65-NF-κB; and K, AP-1. The phosphorylation levels of L, JNK; M, p65-NF-κB; and N, AP-1. $^{\&}P < 0.05$ *vs*. Dex group; $^{\&\&}P < 0.01$ *vs*. Dex group.

3.8 TLR2/4 inhibitors suppressed the anti-inflammatory effects of AJ2-I in LPS-challenged A549 cells

Furthermore, we investigated whether TLR2/4 inhibitors could counteract the anti-inflammatory effects of AJ2-I. IL-6 was randomly chosen for efficacy verification. TLR2 and TLR4 inhibitors suppressed the expression of IL-6 by 46.1% ($P < 0.05$) and 56.3% ($P < 0.01$), respectively (Figure 9A). Notably, the addition of either TLR4 or TLR2 inhibitor could not further reduce IL-6 expression compared to F-H or TLR inhibitor monotherapy. Western blotting results showed consistent results with the gene expression, suggesting that TLR2 or TLR4 inhibitor could counteract the anti-inflammatory effects of AJ2-I (Figure 9E). The detection of the gene expression of TLR2, TLR4 and their downstream gene MyD88 suggested that TLR2 and TLR4 inhibitors had overlapping effects, as TLR4 inhibitor (IAXO-102) inhibited the expression of TLR2 (62.4%, $P < 0.05$), and TLR2 inhibitor (INH14) suppressed the expression of TLR4 (49.5%, $P < 0.01$), while they showed similar effects on inhibition of MyD88 ($P < 0.001$, Figure 9B-D). F-H monotherapy or in combination with either TLR2 or TLR4 inhibitor exhibited similar effects on suppression of these genes. At the protein level, TLR4 and TLR2 inhibitors suppressed TLR2 protein levels by 48.6% ($P < 0.05$) and 59.2% ($P < 0.01$), respectively (Figure 9F), while they inhibited TLR4 protein to a similar level of ~50% ($P < 0.05$, Figure 9G). These results further indicated the non-specific properties of these inhibitors. Consequently, these inhibitors decreased the levels of p-MyD88 protein to a similar extent ($P < 0.01$, Figure 9H). Although the addition of

TLR4 and TLR2 inhibitors further reduced p-MyD88 protein levels by ~30% compared to F-H monotherapy, results exhibited no significant difference. Furthermore, we randomly detected the expression of ERK and p38 involved in the MAPK signaling pathway. Hear again, p38 expression was undetectable (Figure 9J). Both TLR2 and TLR4 inhibitors suppressed the gene expression of ERK (~55% reduction, Figure 9I) and the levels of p-ERK1/2 and p-P38 proteins (~36%-55% reduction, Figure 9M-N). Notably, the addition of these inhibitors could not further decrease the phosphorylation levels of ERK1/2 and P38 compared to F-H monotherapy. At last, both TLR2 and TLR4 inhibitors suppressed the gene expression of p65-NF-κB and AP-1 (Figure 9K-L). The combination groups showed similar inhibitory effects on these two transcriptional factors and exhibited no statistical significance compared to monotherapies. At the protein level, TLR2 and TLR4 inhibitors decreased phosphorylation levels of P65 and AP-1 proteins ($P < 0.05$, Figures 9O-P). Here again, results exhibited no statistical significance among intervention groups.

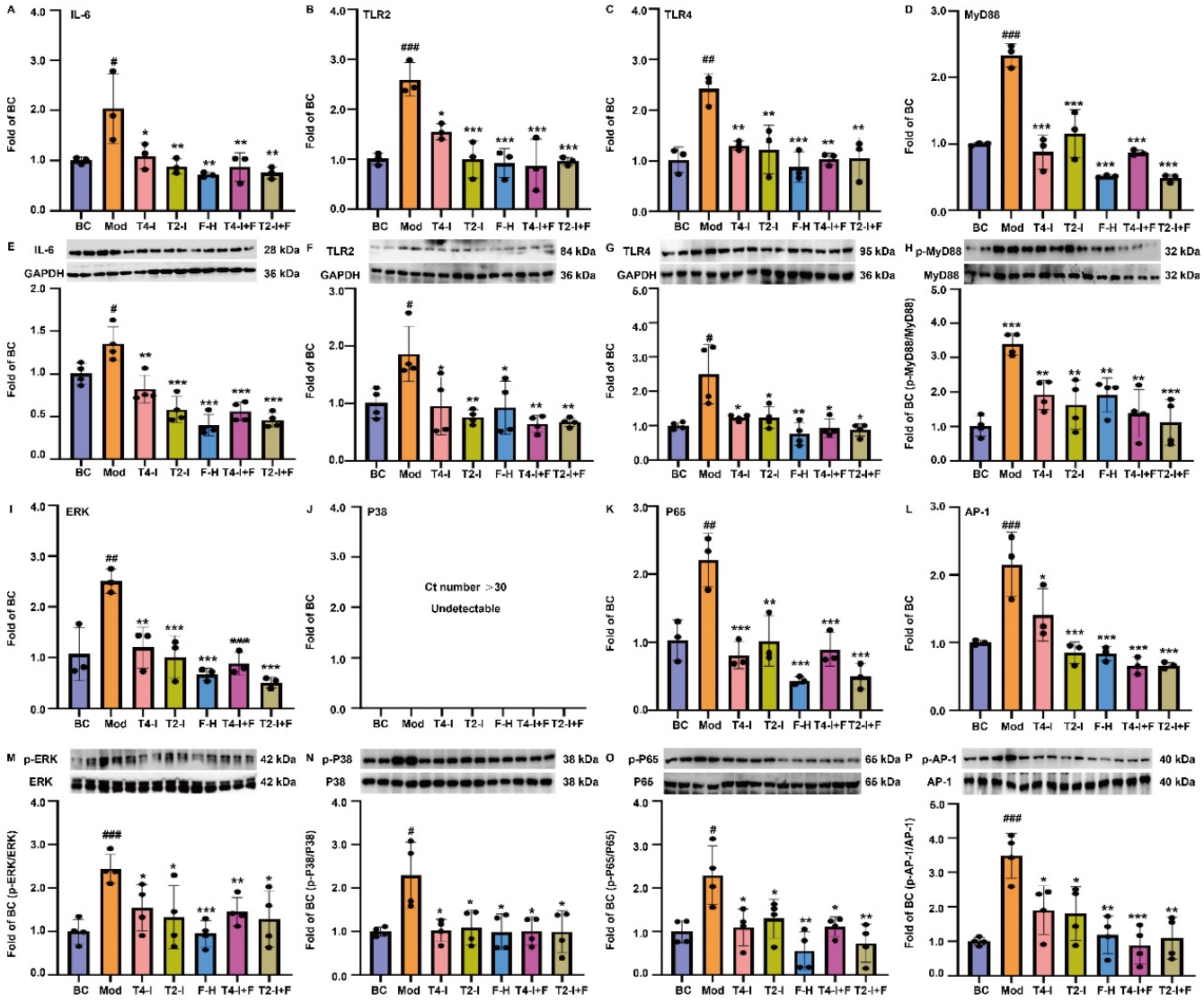

Figure 9. Effects of TLR2 and TLR4 inhibitors (INH14 and IAXO-102) on the anti-inflammatory activities of AJ2-I in A549 cells. The mRNA expression of A, IL-6; B, TLR2; C, TLR4; and D, MyD88 (n=3). The levels of E, IL-6; F, TLR2; G, TLR4; and H, p-MyD88 (n=4). The mRNA expression of I, ERK; J, p38-MAPK; K, p65-NF-κB; and L, AP-1 (n=3). The phosphorylation levels of M, ERK; N, p38-MAPK; O, p65-NF-κB; and P, AP-1 (n=4). T4-I: cells were pre-treated with TLR4 inhibitor (IAXO-102, 4.0 μg/mL) prior to LPS (1.0 μg/mL) challenge; T2-I: cells were pre-treated with TLR2 inhibitor (INH14, 4.0 μg/mL) prior to LPS (1.0 μg/mL) challenge; T4-I+F: cells were pre-treated with TLR4 inhibitor (IAXO-102, 4.0 μg/mL) in combination with AJ-2I (40 μg/mL) prior to LPS (1.0 μg/mL) challenge; T2-I+F: cells were pre-treated with TLR2 inhibitor (INH14, 4.0 μg/mL) in combination with AJ-2I (40 μg/mL) prior to LPS (1.0 μg/mL) challenge.

3.9 TLR2/4 inhibitors suppressed the anti-inflammatory effects of AJ2-I in C57BL/6J mice

Finally, to determine whether the anti-inflammatory effects of AJ2-I are mediated through the TLR2/4 pathway, we administered TLR2/4 inhibitors to LPS-challenged C57BL/6J mice. As shown in Figure 10A-C, LPS challenge significantly elevated the levels of the pro-inflammatory cytokines IL-6, IL-1β, and TNF-α compared to the BC group, whereas Dex treatment markedly suppressed their release. The administration of TLR2/4 inhibitors alone also potently reduced the levels of these cytokines by 51.5% ($P < 0.001$), 34.3% ($P < 0.01$), and 50.8% ($P < 0.01$), respectively. However, the combination of AJ2-I with the inhibitors did not lead to a further significant reduction (Figure 10A-C), suggesting that AJ2-I could not augment the anti-inflammatory effect once TLR2/4 was blocked. Consistently, western blot analysis revealed that the LPS-induced upregulation of TLR2, TLR4, and p-MyD88 proteins was effectively suppressed by both Dex and the TLR2/4 inhibitors (Figure 10D-F). The combination group inhibited the expression of these pathway components by 49.5%, 40.2%, and 54.2%, respectively, which was comparable to the effect of the inhibitors alone. This indicates that the impact of AJ2-I on the TLR2/4 signaling pathway was effectively negated by the inhibitors. Furthermore, the investigation downstream revealed that both the TLR2/4 inhibitors and the combination group similarly suppressed the activation of key signaling nodes, reducing the levels of p-PI3K, p-AKT, p-ERK, and p-P38 by over 61%, 75%, 40%, and 35%, respectively (Figure 10G-J). Both treatments also similarly reduced the phosphorylation of key pro-inflammatory transcription factors, inhibiting p-P65 (NF-κB) and p-AP-1 by over 33% and 54%, respectively (Figure 10K-L). Collectively, these findings suggest that AJ2-I exerts its anti-inflammatory effects primarily through a TLR2/4-dependent pathway.

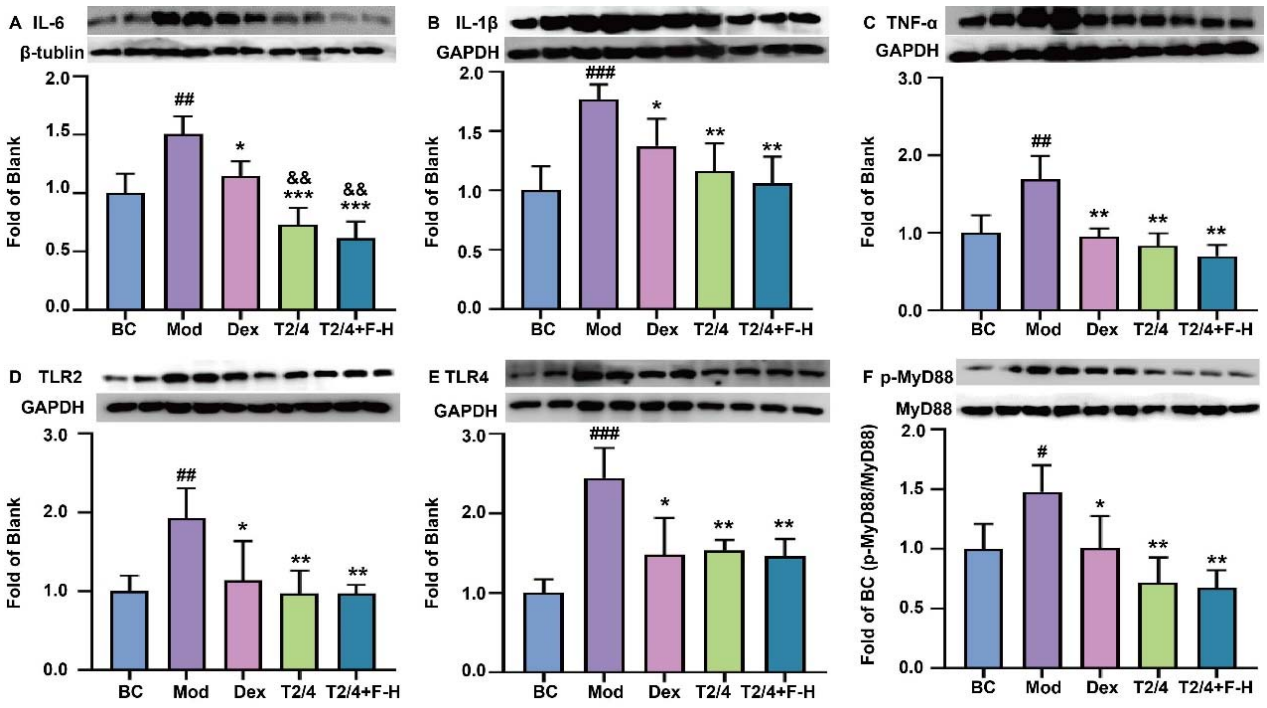

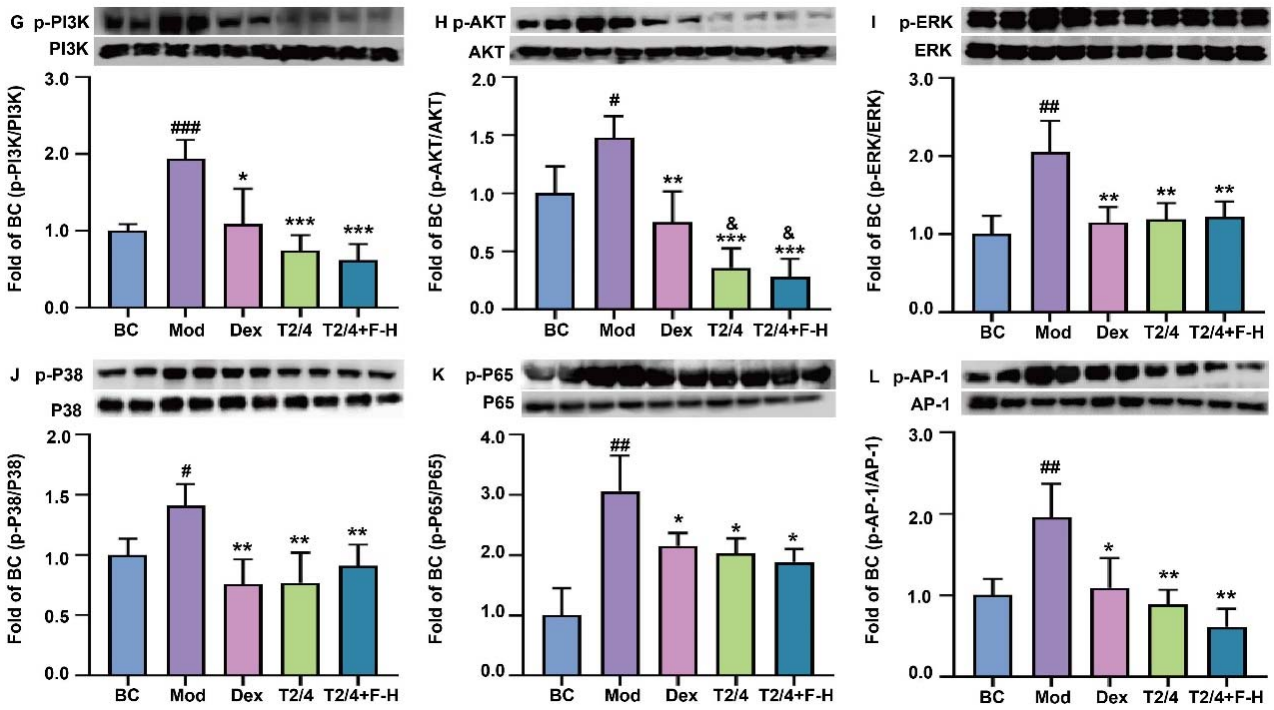

Figure 10. Effects of TLR2 and TLR4 inhibitors (INH14 and IAXO-102) on the anti-inflammatory activities of AJ2-I in C57BL/6J mice. The levels of A, IL-6; B, IL-1β; and C, TNF-α, D, TLR2; E, TLR4; E, p-MyD88; G, p-PI3K; H, p-AKT; I, p-ERK; J, p-P38; K, p-p65-NF-Kb, and L, p-AP-1 (n=4). BC: blank control; Mod: model, the mice were treated with LPS (5.0 mg/kg); Dex: dexamethasone, the mice were first treated with Dex (10 mg/kg) prior to LPS (5.0 mg/kg) challenge; T2/4: the mice were first treated with TLR4 inhibitor (IAXO-102, 3 mg/mL) in combination with TLR2 inhibitor (INH14, 5 mg/mL) prior to LPS (5.0 mg/kg) challenge; T2/4: the mice were first treated with TLR4 inhibitor (IAXO-102, 3 mg/mL) in combination with TLR2 inhibitor (INH14, 5 mg/mL) and high-dosage AJ-2I (200 mg/kg) prior to LPS (5.0 mg/kg) challenge.

4. Discussion

As aforementioned, the urgent need for effective ALI/ARDS therapeutics has highlighted fucoidans as promising candidates, owing to their potent anti-inflammatory properties and favorable oral bioavailability. This is supported by cumulative pharmacokinetic and distribution evidence. For instance, a recent study on *Laminaria japonica* fucoidan (90.8 kDa) reported a maximum serum concentration at 2.8 h and a half-life of 8.8 h[60]. Further supporting this, Pozharitskaya et al. (2018) demonstrated that a high molecular weight fucoidan (735 kDa) could be absorbed in rats, with concentrations peaking in multiple organs around 4 h post-administration[61]. Moreover, *Nagamine* et al. showed that a 28.8 kDa fucoidan was absorbed through the intestine and distributed to the liver, particularly within Küpffer cells[62]. However, the therapeutic potential of sea cucumber-derived fucoidan in ALI mitigation and their precise mechanisms of action remain largely unexplored. Our study addresses this knowledge gape by characterizing the structural properties of *A. japonicus*-derived fucoidan AJ2-I through comprehensive methylation and NMR analysis. Furthermore, we provide novel evidence that AJ2-I effectively attenuates LPS-induced ALI by simultaneously modulating TLR2/4, PI3K/AKT, and MAPK signaling pathways. Crucially, through TLR2/4 inhibition experiments, we demonstrate that AJ2-I's anti-inflammatory effects are predominantly mediated through suppression of the TLR2/4 signaling axis, establishing this pathway as the primary therapeutic target of this marine-derived compound.

Chemically, *A. japonicus*-derived fucoidans exhibit broad compositional ranges: Mw (9~2000 kDa), carbohydrate (20~70%), sulfate (3~36%), and uronic acid (1~16%), influenced by origin and extraction methods[20,21,25,28,53,63,64]. Our analysis of AJ2-I revealed properties consistent with these reports, with its Mw (135.8 kDa) falling within the typical range (25~800 kDa), though notably lower than 1970 kDa reported for Aj-FUC[42]. Like other *A. japonicus*-derived fucoidans, AJ2-I contains minor amounts of neutral sugars (e.g. Man), acidic sugars (e.g. GlcA), and GalNAc[21,25,28,63,65]. Structural analysis using intact samples revealed AJ2-I's characteristic branched structure of [→3)-Fuc*p*-(1→] residues with C4 branching and sulfate groups primarily at C2 and C4 positions. These findings were consistent with previous reported *A. japonicus*-derived fucoidans[25,42,53,66], but distinct from linear fucoidans found in *Holothuria fuscopunctata*, *Thelenota ananas*, and *Stichopus horrens*[20,21,64,66,67]. Although one previous study identified a pentasaccharide repeating unit as the major structure of *A. japonicus*-derived fucoidan, this was based on a degradation product (Mw 105 kDa) generated by the CZ1127 fucoidanase[42]. In their native state, however, fucoidans from *A. japonicas* are generally complex and may not composed of simple repeating unit[20,21]. While *A. japonicus*-derived fucosylated chondroitin sulfate (FCS) has a defined structure →4)-β-D-Glc*p*A-(1→, →3)-β-D-Gal*p*NAC-(1→, and terminal Fuc*p* (1:1:1 ratio) with Fuc*p* linked to Glc*p*A-*O*-3[26,44,64,68], AJ2-I's minor Gal*p*NAc/GlcpA residues do not indicate FCS contamination. First, anion exchange chromatography with sequential NaCl gradients specifically eluted AJ2-I at 2.0 M NaCl (versus 1.0 M for FCS). Second, size-exclusion chromatography confirmed AJ2-I's high purity. Third, previous studies have reported the natural occurrence of GlcpA and GalpNAc residues in *A. japonicus*-derived fucoidans as mentioned in the literatures[20,21,68]. Moreover, AJ2-I contains unique structural features, →4)-β-D-GalpA-6-O-Et-(1→ and →4)-β-D-GalpA-6-OMe-(1→ glycosyls, that are characteristically found in plant polysaccharides[49,50,69], but have not been previously reported in *A. japonicus*-derived carbohydrates, further distinguishing AJ2-I from known *A. japonicus*-derived fucoidan. However, due to heavy overlap of NMR signals and low abundance of some sugars, achieving a full structural elucidation of AJ2-I presented significant challenges.

Functionally, accumulating evidence has demonstrated that both algal and sea cucumber (*A. japonicus*) fucoidans ameliorate LPS-induced cytokine production in RAW264.7 cells, with efficacy strongly linked to their structural characteristics. Notably, fucoidans with higher sulfate content (20-35%) exhibit superior bioactivity, as evidenced by comparative analyses[26,70,71]. Mw similarly influences efficacy, with lower-Mw fucoidans (e.g., 63.2 versus 124.5 kDa, from *A. nodosum*) demonstrating greater anti-inflammatory effects compared to higher-Mw equivalents[72-74]. Furthermore, uronic acid might play a role. For instance, *Cystoseira crinite*-derived fucoidan (13.15% uronic acid, 17.00% sulfates) effectively reduced inflammation in a rat model[75]. Our findings with *A. japonicus*-derived AJ2-I (135.8 kDa, 13.0% GlcA, 27.0% sulfate) corroborate these structure-activity relationships, showing both superior ALI attenuation and greater potency (10 versus 50 μg/mL effective dose) compared to a higher-Mw (1970 kDa), lower-sulfate (23.3%) variant[76]. Structural analyses reveal high branched fucoidans exhibit robust efficacy. For instance, *Fucus vesiculosus*-derived fucoidan with alternative →3)-α-L-Fuc*p*2(SO_3^-)-(1→4)-α-L-Fuc*p*2,3(SO_3^-)$_2$-(1→ linked

glycosyls ameliorated hyperoxic lung injury[77], and orally administration of *U. pinnatifida*-derived fucoidan successfully reduced mice lung consolidation, particularly when the animals were pre-treated with fucoidan[78]. Consistently, *A. nodosum* fucoidan with higher branching degree showed better effects on attenuating SARS-CoV-2 infection than *U. pinnatifida*-derived fucoidan with lower branching degree[79]. Other high branched *A. nodosum*-derived fucoidans also exhibited robust anti-inflammatory effects[73].

Currently, the mechanisms by which fucoidan exerts its protective effects against ALI remain unclear. Notably, TLRs are specific type I transmembrane proteins that play a critical role in ALI/ARDS by triggering key inflammatory pathways, including NF-κB and MAPK, particularly upon LPS stimulation[2,3,5,**80**]. This study demonstrated that AJ2-I reduced the gene and protein levels of TLR2 and TLR4. Consistently, *A. japonicas*-derived fucoidan suppressed the TLR4/NF-κB signaling pathway[76], *A. nodosum*-derived fucoidans (63.2 and 124.5 kDa) attenuated the expression of TLR2/4[73], and *Padina commersonii*-derived fucoidan (50-200 μg/mL) containing 65.8% fucose and 27.51% sulfate decreased the expression of TLR2/4 and MyD88[81], in LPS-induced macrophages. Another *A. nodosum*-derived fucoidan with alternating (1→3) and (1→4) linked Fuc*p* residues (18.94 kDa, 17% sulfate) inhibited TLR3-induced cytokine release[82]. These findings suggest the critical role of TLRs in fucoidan-mediated anti-inflammatory mechanisms.

Moreover, the MAPK and PI3K/AKT signaling pathways play crucial roles in inflammatory processes by activating transcriptional factors and interacting with TLR signaling[83]. Our study demonstrated that fucoidan AJ2-I down-regulated phosphorylation of PI3K/AKT and MAPK family members. These findings align with previous reports by algal fucoidans showing: (1) *U. pinnatifida*-derived fucoidan (10-200 μg/mL) suppresses PI3K/AKT and p38-MAPK phosphorylation, inducing apoptosis in A549 cells[84]; (2) *F. vesiculosus* fucoidan inhibits PI3K/AKT and MAPK/NF-κB pathways, reducing A549 cell migration and invasion[85]; (3) another *F. vesiculosus* fucoidan attenuates hyperoxic lung injury by blocking ERK1/2 phosphorylation[77]; and (4) *S. japonica* fucoidan (30.72% sulfate, 79.49% fucose) suppresses inflammation through MAPK/NF-κB pathway inhibition in LPS-stimulated macrophages[71]. Furthermore, MAPK activation promotes inflammatory mediators, cyclooxygenase-2 and inducible nitric oxide synthase, whose activities are suppressed upon fucoidan treatment[70,71,73,82]. Collectively, we demonstrate that AJ2-I suppresses ALI through inhibition of TLR2/4, PI3K/AKT, and MAPK signaling pathways and provide novel evidence that AJ2-I targets AP-1 transcription, extending beyond the well-characterized NF-κB pathway. Crucially, we demonstrate that AJ2-I exerts its protective effects predominantly via TLR2/4-mediated signaling. This conclusion is supported by the effective suppression of its anti-inflammatory activity —along with the inhibition of PI3K/AKT and MAPK pathways—upon treatment with TLR2/4 antagonists. Importantly, these findings suggest that AJ2-I's therapeutic benefits derive from its optimal Mw, sulfate and uronic acid content combined with its [→3)-Fuc*p*-(1→] branched architecture, exemplifying how structural features govern fucoidan bioactivity.

However, a thorough assessment of chronic toxicity and off-target effects is a critical prerequisite for advancing this fucoidan toward therapeutic application. Equally important is the consideration of sex as a

biological variable, given the increasing evidence of sex-specific inflammatory responses in murine models. For instance, lung cytokine expression (IL-1β, TNF-α, IL-6) following woodsmoke exposure was shown to be sex-dependent[86]. Similarly, ozone-induced lung inflammation triggered sex-specific microRNA expression networks[87], and a ketogenic diet exerted stronger effects on lung immunity in males[88]. Therefore, future studies must specifically investigate whether the anti-inflammatory efficacy of AJ2-I is influenced by sex.

5. Conclusions

We isolated a novel fucoidan, AJ2-I, from sea cucumber *A. japonicas*. It primarily consists of [→3)-Fuc*p*-(1→] backbone with branching at C4 positions, while sulfate groups were predominantly substituted at C2 and C4 positions. This fucoidan differs from the previously reported *A. japonicus*-derived polysaccharides due to the presence of unique glycosyl residues, including →4)-β-D-Gal*p*A-6-O-Et-(1→ and →4)-β-D-Gal*p*A-6-OMe-(1→. Notably, AJ2-I attenuated LPS-induced ALI *in vivo* and *in vitro*. Mechanistically, it suppressed TLR2/4 activation and downstream signaling pathways, including MAPK and PI3K/AKT, leading to inactivation of key transcriptional factors (NF-κB and AP-1). Collectively, these findings demonstrate the protective role of *A. japonicas*-derived fucoidan in ALI and elucidate its underlying anti-inflammatory mechanisms, thus providing a promising foundation for developing fucoidan-based therapies against lung inflammation, including ALI.

Acknowledgements

This work was supported by National Natural Science Foundation of China (82070469).

Data availability

The raw data used in this article are attached as Supplementary Materials.

Declaration of competing interest

None.

References

[1] V. Kumar, Pulmonary innate immune response determines the outcome of inflammation during pneumonia and sepsis-associated acute lung injury, Front. Immunol. 11 (2020) 1722. https://doi.org/10.3389/fimmu.2020.01722.

[2] K.A. Shirey, J.C.G. Blanco, S.N. Vogel, Targeting TLR4 signaling to blunt viral-mediated acute lung injury, Front. Immunol. 12 (2021) 705080. https://doi.org/10.3389/fimmu.2021.705080.

[3] M.E. Long, R.K. Mallampalli, J.C. Horowitz, Pathogenesis of pneumonia and acute lung injury, Clin. Sci. (Lond) 136 (2022) 747-769. https://doi.org/10.1042/cs20210879.

[4] J. Xiao, L. Wang, B. Zhang, et al., Cell death in acute lung injury: caspase-regulated apoptosis, pyroptosis, necroptosis, and PANoptosis, Front. Pharmacol. 16 (2025) 1559659. https://doi.org/10.3389/fphar.2025.1559659.

[5] Y.Q. He, C.C. Zhou, L.Y. Yu, et al., Natural product derived phytochemicals in managing acute lung injury by multiple mechanisms, Pharmacol. Res. 163 (2021) 105224. https://doi.org/10.1016/j.phrs.2020.105224.

[6] S.M. Vora, J. Lieberman, H. Wu, Inflammasome activation at the crux of severe COVID-19, Nat. Rev. Immunol. 21 (2021) 694-703. https://doi.org/10.1038/s41577-021-00588-x.

[7] N.E. Ingraham, A.G. Barakat, R. Reilkoff, et al., Understanding the renin-angiotensin-aldosterone-SARS-CoV axis: a comprehensive review, Eur. Respir. J. 56 (2020) https://doi.org/10.1183/13993003.00912-2020.

[8] C. Lee, W.J. Choi, Overview of COVID-19 inflammatory pathogenesis from the therapeutic perspective, Arch. Pharm. Res. 44 (2021) 99-116. https://doi.org/10.1007/s12272-020-01301-7.

[9] N.T. Mowery, W.T.H. Terzian, A.C. Nelson, Acute lung injury, Curr. Probl. Surg. 57 (2020) 100777. https://doi.org/10.1016/j.cpsurg.2020.100777.

[10] G. Ding, X. Zhang, A. Vinturache, et al., Challenges in the treatment of pediatric *Mycoplasma pneumoniae* pneumonia, Eur. J. Pediatr. 183 (2024) 3001-3011. https://doi.org/10.1007/s00431-024-05519-1.

[11] S. Lakshmana Senthil, A comprehensive review to assess the potential, health benefits and complications of fucoidan for developing as functional ingredient and nutraceutical, Int. J. Biol. Macromol. 277 (2024) 134226. https://doi.org/10.1016/j.ijbiomac.2024.134226.

[12] Z. Qu, H. Li, F. Qiang, et al., Regulation of inflammation by Chaihu-Shugan-San: targeting the IL-17/ NF-κB pathway to combat breast cancer-related depression, Phytomedicine 143 (2025) 156836. https://doi.org/10.1016/j.phymed.2025.156836.

[13] Y.K. Xie, X.Y. Pan, X.R. Liang, et al., Research progress on structural characterization and bioactivities of *Poria cocos and Ganoderma* polysaccharides, Food & Medicine Homology 2 (2025) 9420040. https://doi.org/10.26599/FMH.2025.9420040.

[14] Z.X. Li, M. Zhang, Y.Y. Liu, et al., Advances in the preparation, structure-activity relationship, and biological mechanisms of *Agaricus Polysaccharides*, Food Sci. Hum. Wellness (2025) 9250590. https://doi.org/10.26599/FSHW.2025.9250590.

[15] Z.X. Wang, K. Huang, K.L. Pu, et al., Naematelia aurantialba: a comprehensive review of its medicinal, nutritional, and cultivation aspects, Food & Medicine Homology 2 (2025) 9420072. https://doi.org/10.26599/FMH.2025.9420072.

[16] Y.Y. Yu, Y.N. Duan, S. Ma, et al., Research progress on the mechanism of functional activity of edible fungi polysaccharides—focusing intestinal mucus as a key and entry point, Food & Medicine Homology 2 (2025) 9420042. https://doi.org/10.26599/FMH.2025.9420042.

[17] E. Apostolova, P. Lukova, A. Baldzhieva, et al., Immunomodulatory and anti-inflammatory effects of fucoidan: A Review, Polymers (Basel) 12 (2020) https://doi.org/10.3390/polym12102338.

[18] M. Matin, M. Koszarska, A.G. Atanasov, et al., Bioactive potential of algae and algae-derived compounds: focus on anti-inflammatory, antimicrobial, and antioxidant effects, Molecules 29 (2024) https://doi.org/10.3390/molecules29194695.

[19] S.R. Shi, J.W. Xin, H.H. Ji, et al., The combination of *Fucus vesiculosus*-derived fucoidan and simvastatin attenuates atherosclerosis induced by a high-fat diet plus balloon catheter injury in New Zealand rabbits, Int. J. Biol. Macromol. 320 (2025) 145628. https://doi.org/10.1016/j.ijbiomac.2025.145628.

[20] G. Chen, L. Yu, F. Shi, et al., A comprehensive review of sulfated fucan from sea cucumber: antecedent and prospect, Carbohydr. Polym. 341 (2024) 122345. https://doi.org/10.1016/j.carbpol.2024.122345.

[21] A. Hossain, D. Dave, F. Shahidi, Sulfated polysaccharides in sea cucumbers and their biological properties: a review, Int. J. Biol. Macromol. 253 (2023) 127329. https://doi.org/10.1016/j.ijbiomac.2023.127329.

[22] J. Zhou, Z. Peng, J. Wang, Trelagliptin alleviates lipopolysaccharide (lps)-induced inflammation and oxidative stress in acute lung injury mice, Inflammation 44 (2021) 1507-1517. https://doi.org/10.1007/s10753-021-01435-w.

[23] G. Matute-Bello, C.W. Frevert, T.R. Martin, Animal models of acute lung injury, Am. J. Physiol. Lung Cell Mol. Physiol. 295 (2008) L379-399. https://doi.org/10.1152/ajplung.00010.2008.

[24] J.Y Yin, X.Q Yang, B. Xia, et al., The fucoidan from sea cucumber *Apostichopus japonicus* attenuates lipopolysaccharide-challenged liver injury in C57BL/6J mice, J. Funct. Foods 61 (2019) 103493.

[25] J. Ye, L. Zheng, W. Pan, et al., Sulfated polysaccharide from *Apostichopus japonicus* viscera exhibits anti-inflammatory properties *in vitro* and *in vivo*, Int. J. Biol. Macromol. 280 (2024) 135500. https://doi.org/10.1016/j.ijbiomac.2024.135500.

[26] A. Staub, Removal of protein-Sevag method. Methods Carbohydr Chem. 5(2) (1965) 5–6.

[27] P.X. Gong, Q.Y. Li, Y.C. Wu, et al., Structural elucidation and antidiabetic activity of fucosylated chondroitin sulfate from sea cucumber *Stichopus japonicas*, Carbohydr. Polym. 262 (2021) 117969. https://doi.org/10.1016/j.carbpol.2021.117969.

[28] D. Yang, F. Lin, Y. Huang, et al., Separation, purification, structural analysis and immune-enhancing activity of sulfated polysaccharide isolated from sea cucumber viscera, Int. J. Biol. Macromol. 155 (2020) 1003-1018. https://doi.org/10.1016/j.ijbiomac.2019.11.064.

[29] C.F. Ji, Z.R. Zhang, B.H. Zhang, et al., Purification, characterization, and *in vitro* antitumor activity of a novel glucan from the purple sweet potato *Ipomoea Batatas (L.)* Lam, Carbohydr. Polym. 257 (2021) 117605. https://doi.org/10.1016/j.carbpol.2020.117605.

[30] M. DuBois, K.A. Gilles, J.K. Hamilton, et al., Colorimetric method for determination of sugars and related substances. Anal. Chem. 28(3) (1956) 350-356.

[31] T. Bitter, H.M. Muir, A modified uronic acid carbazole reaction. Analyt. Biochemistry 4(4) (1962) 330-334. https://doi.org/10.1016/0003-2697(62)90095-7.

[32] X. Wang, S.R. Shi, M.M. Sun, et al., Mechanisms of action of *Fucus vesiculosus*-derived fucoidan on improving dyslipidemia in New Zealand rabbits fed a high-fat diet, Int. J. Biol. Macromol. 314 (2025) 144148. https://doi.org/10.1016/j.ijbiomac.2025.144148.

[33] J. Wang, Y. Wang, X. Yang, et al., Purification, structural characterization, and PCSK9 secretion inhibitory effect of the novel alkali-extracted polysaccharide from *Cordyceps militaris*, Int. J. Biol. Macromol. 179 (2021) 407-417. https://doi.org/10.1016/j.ijbiomac.2021.02.191.

[34] X.Y. Yang, P.L. Lin, J.Z. Wang, et al., Purification, characterization and anti-atherosclerotic effects of the polysaccharides from the fruiting body of *Cordyceps militaris*, Int. J. Biol. Macromol. 181 (2021) 890-904. https://doi.org/10.1016/j.ijbiomac.2021.04.083.

[35] S. Ma, W. Song, Y. Xu, et al., Neutralizing tumor-promoting inflammation with polypeptide-dexamethasone conjugate for microenvironment modulation and colorectal cancer therapy, Biomaterials 232 (2020) 119676. https://doi.org/10.1016/j.biomaterials.2019.119676.

[36] C. Huggins, S. Pearce, F. Peri, et al., A novel small molecule TLR4 antagonist (IAXO-102) negatively regulates non-hematopoietic toll like receptor 4 signalling and inhibits aortic aneurysms development, Atherosclerosis 242 (2015) 563-570. https://doi.org/10.1016/j.atherosclerosis.2015.08.010.

[37] M. Drexel, J. Kirchmair, S. Santos-Sierra, INH14, a small-molecule urea derivative, inhibits the IKKalpha/beta-dependent TLR inflammatory response, chembiochem. 20 (2019) 710-717. https://doi.org/10.1002/cbic.201800647.

[38] M. Miao, X.Y. Zhang, H.X. Yu, et al., Mechanisms underlying the effects of the conditional knockdown of hepatic PCSK9 in attenuating lipopolysaccharide-induced acute liver inflammation, Int. J. Biol. Macromol. 291 (2025) 139066. https://doi.org/10.1016/j.ijbiomac.2024.139066.

[39] H.G. Lee, H. Jayawardhana, F. Yang, et al., Fucoidan from *Myelophycus caespitosus* attenuates inflammation by regulating pro-inflammatory cytokines and NF-κB signaling in LPS-induced RAW 264.7 macrophages, Food Sci. Biotechnol. 34 (2025) 1453-1465. https://doi.org/10.1007/s10068-024-01743-5.

[40] A. Ma, J. Zhou, H. Zou, et al., Anti-inflammatory effect of nestorone in a lipopolysaccharide-induced acute lung injury model through regulation of the TLR-4/Myd88/NF-κB signaling pathway, Inflammopharmacology 33 (2025) 1473-1489. https://doi.org/10.1007/s10787-024-01625-6.

[41] J.S.Y. Tam, J.K. Coller, P.A. Hughes, et al., Toll-like receptor 4 (TLR4) antagonists as potential therapeutics for intestinal inflammation, Indian J. Gastro. 40 (2021) 5-21. https://doi.org/10.1007/s12664-020-01114-y.

[42] L. Yu, C. Xue, Y. Chang, et al., Structure and rheological characteristics of fucoidan from sea cucumber *Apostichopus japonicus*, Food Chem. 180 (2015) 71-76. https://doi.org/10.1016/j.foodchem.2015.02.034.

[43] O. Yuliarti, S.Y. Chong, K.K.T. Goh, Physicochemical properties of pectin from green jelly leaf (*Cyclea barbata Miers*), Int. J. Biol. Macromol. 103 (2017) 1146-1154. https://doi.org/10.1016/j.ijbiomac.2017.05.147.

[44] N.E. Ustyuzhanina, M.I. Bilan, A.S. Dmitrenok, et al., Structure and biological activity of a fucosylated chondroitin sulfate from the sea cucumber *Cucumaria japonica*, Glycobiology. 26 (2016) 449-459. https://doi.org/10.1093/glycob/cwv119.

[45] J.J. Kenyon, S.Y.N. Senchenkova, A.S. Shashkov, et al., K17 capsular polysaccharide produced by *Acinetobacter baumannii* isolate G7 contains an amide of 2-acetamido-2-deoxy-d-galacturonic acid with d-alanine, Int. J. Biol. Macromol. 144 (2020) 857-862. https://doi.org/10.1016/j.ijbiomac.2019.09.163.

[46] N.E. Ustyuzhanina, M.I. Bilan, A.S. Dmitrenok, et al., Fucosylated chondroitin sulfates from the sea cucumbers *Paracaudina chilensis* and *Holothuria hilla*: Structures and anticoagulant activity, Mar. Drugs 18 (2020) https://doi.org/10.3390/md18110540.

[47] F. Xiong, H.Y. Li, H.L. Yao, et al., A galacturonic acid-rich polysaccharide from *Citrus medica* 'fingered' alleviated the dextran sulfate sodium-induced ulcerative colitis, Int. J. Biol. Macromol. 294 (2025) 139506. https://doi.org/10.1016/j.ijbiomac.2025.139506.

[48] Y. Cui, R. Wang, S. Cao, et al., A galacturonic acid-rich polysaccharide from *Diospyros kaki* peel: Isolation, characterization, rheological properties and antioxidant activities *in vitro*, Food Chem. 416 (2023) 135781. https://doi.org/10.1016/j.foodchem.2023.135781.

[49] C.W. Huang, Y.C. Chen, T.C. Yin, et al., Low-molecular-weight fucoidan as complementary therapy of fluoropyrimidine-based chemotherapy in colorectal cancer, Int. J. Mol. Sci. 22 (2021) https://doi.org/10.3390/ijms22158041.

[50] Z. Manafu, R. Du, T. Kudereti, et al., Structure characterization and intestinal immune promotion effect of polysaccharide purified from *Alhagi camelorum* Fisch, Int. J. Biol. Macromol. 269 (2024) 132077. https://doi.org/10.1016/j.ijbiomac.2024.132077.

[51] Y.L. Cui, S.Y. Cao, X. Wang, et al., Characterization of a pectic heteropolysaccharide isolated from persimmon peel and its anti-inflammatory activity, Food Sci. Hum. Wellness (2025) 9250473, https://doi.org/10.26599/FSHW.2025.9250473.

[52] M.I. Bilan, A.A. Grachev, A.S. Shashkov, et al., Further studies on the composition and structure of a fucoidan preparation from the brown alga *Saccharina latissima*, Carbohydr. Res. 345 (2010) 2038-2047. https://doi.org/10.1016/j.carres.2010.07.009.

[53] Y. Kariya, B. Mulloy, K. Imai, et al., Isolation and partial characterization of fucan sulfates from the body wall of sea cucumber *Stichopus japonicus* and their ability to inhibit osteoclastogenesis, Carbohydr. Res. 339 (2004) 1339-1346. https://doi.org/10.1016/j.carres.2004.02.025.

[54] M.I. Bilan, N.E. Ustyuzhanina, A.S. Shashkov, et al., A sulfated galactofucan from the brown alga *Hormophysa cuneiformis (Fucales, Sargassaceae)*, Carbohydr. Res. 469 (2018) 48-54. https://doi.org/10.1016/j.carres.2018.09.001.

[55] R.B. Jia, G. Yang, H. Lai, et al., Structural characterization and human gut microbiota fermentation in vitro of a polysaccharide from *Fucus vesiculosus*, Int, J, Biol. Macromol. 275 (2024) 133369. https://doi.org/10.1016/j.ijbiomac.2024.133369.

[56] A. Khamleng, G. Chen, J. Shen, et al., Structural analysis of sulfated fucan from the sea cucumber *Holothuria mexicana* with the assistance of endo-1,3-fucanase, Carbohydr. Polym. 352 (2025) 123231. https://doi.org/10.1016/j.carbpol.2025.123231.

[57] X. Shi, R. Guan, L. Zhou, et al., Structural characterization and heparanase inhibitory activity of fucosylated glycosaminoglycan from *Holothuria floridana*, Mar. Drugs 19 (2021) https://doi.org/10.3390/md19030162.

[58] M.I. Bilan, N.E. Ustyuzhanina, A.S. Shashkov, et al., Sulfated polysaccharides of the *Vietnamese brown* alga *Sargassum aquifolium (Fucales, Sargassaceae)*, Carbohydr. Res. 449 (2017) 23-31. https://doi.org/10.1016/j.carres.2017.06.016.

[59] X. Yang, P. Lin, J. Wang, et al., Purification, characterization and anti-atherosclerotic effects of the polysaccharides from the fruiting body of *Cordyceps militaris*, Int. J. Biol. Macromol. 181 (2021) 890-904. https://doi.org/10.1016/j.ijbiomac.2021.04.083.

[60] X.N. Sun, C.H. Yan, Y.H. Fu, et al., Orally administrated fucoidan and its low-molecular-weight derivatives are absorbed differentially to alleviate coagulation and thrombosis. Int. J. Biol. Macromol. 255 (2024) 128092. https://doi.org/10.1016/j.ijbiomac.2023.128092.

[61] O.N. Pozharitskaya, A.N. Shikov, N.M. Faustova, et al., Pharmacokinetic and tissue distribution of fucoidan from *Fucus vesiculosus* after oral administration to rats. Mar. Drugs 16(4) (2018) 132. https://doi.org/10.3390/md16040132.

[62] T. Nagamine, K. Nakazato, S. Tomioka, et al., Intestinal absorption of fucoidan extracted from the brown seaweed, *Cladosiphon okamuranus*, Mar. Drugs 13 (2015) 48–64, https://doi.org/10.3390/md13010048.

[63] U. Surayot, S. Lee, S. You, Effects of sulfated fucan from the sea cucumber *Stichopus japonicus* on natural killer cell activation and cytotoxicity, Int. J. Biol. Macromol. 108 (2018) 177-184. https://doi.org/10.1016/j.ijbiomac.2017.11.102.

[64] L. Luo, M. Wu, L. Xu, et al., Comparison of physicochemical characteristics and anticoagulant activities of polysaccharides from three sea cucumbers, Mar. Drugs 11 (2013) 399-417. https://doi.org/10.3390/md11020399.

[65] Y. Li, Y. Huan, W. Qin, et al., Fucoidan from *Apostichopus japonicus* ameliorates alcoholic liver disease by regulating gut-liver axis homeostasis, Int. J. Biol. Macromol. 270 (2024) 132093. https://doi.org/10.1016/j.ijbiomac.2024.132093.

[66] R.A. Cao, U. Surayot, S. You, Structural characterization of immunostimulating protein-sulfated fucan complex extracted from the body wall of a sea cucumber, *Stichopus japonicus*, Int. J. Biol. Macromol. 99 (2017) 539-548. https://doi.org/10.1016/j.ijbiomac.2017.03.026.

[67] F. Shang, R. Mou, Z. Zhang, et al., Structural analysis and anticoagulant activities of three highly regular fucan sulfates as novel intrinsic factor Xase inhibitors, Carbohydr. Polym. 195 (2018) 257-266. https://doi.org/10.1016/j.carbpol.2018.04.117.

[68] C. Lu, X. Wang, J. Ma, et al., Chemical substances and their activities in sea cucumber *Apostichopus japonicus*: a review, Arch. Pharm. (Weinheim) 357 (2024) e2300427. https://doi.org/10.1002/ardp.202300427.

[69] X.S. Wang, J.F. Gan, M.H. Han, et al., Comparison of structure and the synergistic anti-hepatocellular carcinoma effect of three polysaccharides from vinegar-baked *Radix Bupleuri*, Int. J. Biol. Macromol. 282 (2024) 136755. https://doi.org/10.1016/j.ijbiomac.2024.136755.

[70] I.P. Shanura Fernando, K.K. Asanka Sanjeewa, K.W. Samarakoon, et al., A fucoidan fraction purified from *Chnoospora minima*; a potential inhibitor of LPS-induced inflammatory responses, Int. J. Biol. Macromol. 104 (2017) 1185-1193. https://doi.org/10.1016/j.ijbiomac.2017.07.031.

[71] L. Ni, L. Wang, X. Fu, et al., *In vitro* and *in vivo* anti-inflammatory activities of a fucose-rich fucoidan isolated from *Saccharina japonica*, Int. J. Biol. Macromol. 156 (2020) 717-729. https://doi.org/10.1016/j.ijbiomac.2020.04.012.

[72] H.D. Liu, D.Y. Ma, S.R. Shi, et al., Preparation and bioactivities of low-molecular weight fucoidans and fuco-oligosaccharides: a review, Carbohydr. Polym. 356 (2025) 123377. https://doi.org/10.1016/j.carbpol.2025.123377.

[73] L.L. Wang, L.L.Wang, C.H. Yan, et al., Two *Ascophyllum nodosum* fucoidans with different molecular weights inhibit inflammation via blocking of TLR/NF-κB signaling pathway discriminately, Foods 11 (2022) https://doi.org/10.3390/foods11152381.

[74] M. Chen, J. Wang, P. Zhang, et al., Low molecular weight fucoidan induces M2 macrophage polarization to attenuate inflammation through activation of the AMPK/mTOR autophagy pathway, Eur J Pharmacol. 986 (2024) 177134. https://doi.org/10.1016/j.ejphar.2024.177134.

[75] E. Apostolova, P. Lukova, A. Baldzhieva, et al., Structural characterization and *in vivo* anti-inflammatory activity of fucoidan from *Cystoseira crinita (Desf.)* Borry, Mar. Drugs 20 (2022) https://doi.org/10.3390/md20110714.

[76] T. Hou, X. Liu, S. Zhang, et al., Anti-inflammatory effects of the fucoidan from sea cucumber *Apostichopus japonicus*, Mar. Biotechnol. (NY) 27 (2025) 32. https://doi.org/10.1007/s10126-025-10410-7.

[77] M. Nie, Y. Wang, Y. Lu, et al., Protective effects of fucoidan against hyperoxic lung injury via the ERK signaling pathway, Mol. Med. Rep. 17 (2018) 1813-1818. https://doi.org/10.3892/mmr.2017.8022.

[78] C. Richards, N.A. Williams, J.H. Fitton, et al., Oral fucoidan attenuates lung pathology and clinical signs in a severe influenza a mouse model, Mar. Drugs 18 (2020) https://doi.org/10.3390/md18050246.

[79] F.S. Shi, Y.H. Xie, Y.L. Yang, et al., Fucoidan from *Ascophyllum nodosum* and *Undaria pinnatifida* attenuate SARS-CoV-2 infection *in vitro* and *in vivo* by suppressing ACE2 and alleviating inflammation, Carbohydr. Polym. 332 (2024) 121884. https://doi.org/10.1016/j.carbpol.2024.121884.

[80] Y.K. Xie, X.Y. Pan, X.R. Liang, et al., Research progress on structural characterization and bioactivities of *Poria cocos and Ganoderma* polysaccharides, Food & Medicine Homology 2 (2025) 9420040. https://doi.org/10.26599/FMH.2025.9420040.

[81] K.K. Asanka Sanjeewa, T.U. Jayawardena, H.S. Kim, et al., Fucoidan isolated from *Padina commersonii* inhibit LPS-induced inflammation in macrophages blocking TLR/NF-κB signal pathway, Carbohydr. Polym. 224 (2019) 115195. https://doi.org/10.1016/j.carbpol.2019.115195.

[82] M. Dutot, S. Grassin-Delyle, H. Salvator, et al., A marine-sourced fucoidan solution inhibits Toll-like-receptor-3-induced cytokine release by human bronchial epithelial cells, Int. J. Biol. Macromol. 130 (2019) 429-436. https://doi.org/10.1016/j.ijbiomac.2019.02.113.

[83] O.F. Fagbohun, W. Thilakarathna, J. Zhou, et al., Sea cucumber and blueberry extracts suppress inflammation and reduce acute lung injury through the regulation of NF-κB/MAPK/JNK signaling pathway in lipopolysaccharide-treated C57BL/6 Mice, Molecules 29 (2024) https://doi.org/10.3390/molecules29071511.

[84] H.J. Boo, J.H. Hyun, S.C. Kim, et al., Fucoidan from *Undaria pinnatifida* induces apoptosis in A549 human lung carcinoma cells, Phytother. Res. 25 (2011) 1082-1086. https://doi.org/10.1002/ptr.3489.

[85] H. Lee, J.S. Kim, E. Kim, Fucoidan from seaweed *Fucus vesiculosus* inhibits migration and invasion of human lung cancer cell via PI3K-Akt-mTOR pathways, PLoS One 7 (2012) e50624. https://doi.org/10.1371/journal.pone.0050624.

[86] K. Wardhani, S. Yazzie, C. McVeigh, et al., Systemic immunological responses are dependent on sex and ovarian hormone presence following acute inhaled woodsmoke exposure. Part. Fibre. Toxicol. 21(1) (2024) 27. https://doi.org/10.1186/s12989-024-00587-5.

[87] N. Fuentes, A. Roy, V. Mishra, et al., Sex-specific microRNA expression networks in an acute mouse model of ozone-induced lung inflammation. Biol. Sex. Differ. 9(1) (2018) 18. https://doi.org/10.1186/s13293-018-0177-7.

[88] C.D. Ekpruke, O. Borges-Sosa, C.A. Hassel, et al., Sex-specific anti-inflammatory effects of a ketogenic diet in a mouse model of allergic airway inflammation. Int. J. Mol. Sci. 26(7) (2025) 3046. https://doi.org/10.3390/ijms26073046.